1 **Comparative removal of As(V) and Sb(V) from aqueous solution by sulfide-**

2 **modified α-FeOOH**

3

4 Qiao Li[a], Rui Li[a], Xinyue Ma[a], Binoy Sarkar[b*], Xiuyun Sun[a¶], Nanthi Bolan[c]

5

6 [a] Jiangsu Key Laboratory of Chemical Pollution Control and Resources Reuse, School

7 of Environmental and Biological Engineering, Nanjing University of Science and

8 Technology, Nanjing 210094, China

9 [b] Lancaster Environment Centre, Lancaster University, Lancaster, LA1 4YQ, United

10 Kingdom

11 [c] Global Centre for Environmental Remediation, University of Newcastle, Callaghan

12 Campus, NSW 2308, Australia

13

14 [*]Corresponding author: Dr. Binoy Sarkar; Lancaster University; e-mail:

15 b.sarkar@lancaster.ac.uk; and

16 [¶]Co-corresponding author: Prof. Xiuyun Sun; Nanjing University of Science and

17 Technology; e-mail: sunxyun@njust.edu.cn

**Highlights**

- Sulfide-modified α-FeOOH was synthesized for As(V) and Sb(V) removal.

- As(V)/Sb(V) adsorption capacity and affinity were remarkably improved.

- Enhanced removal was maintained at pH range from 2 to 11.

- Reduction of As(V) to As(III) followed by adsorption was identified.

- Removal was not affected by the presence of coexisting anions.

**Graphical abstract**
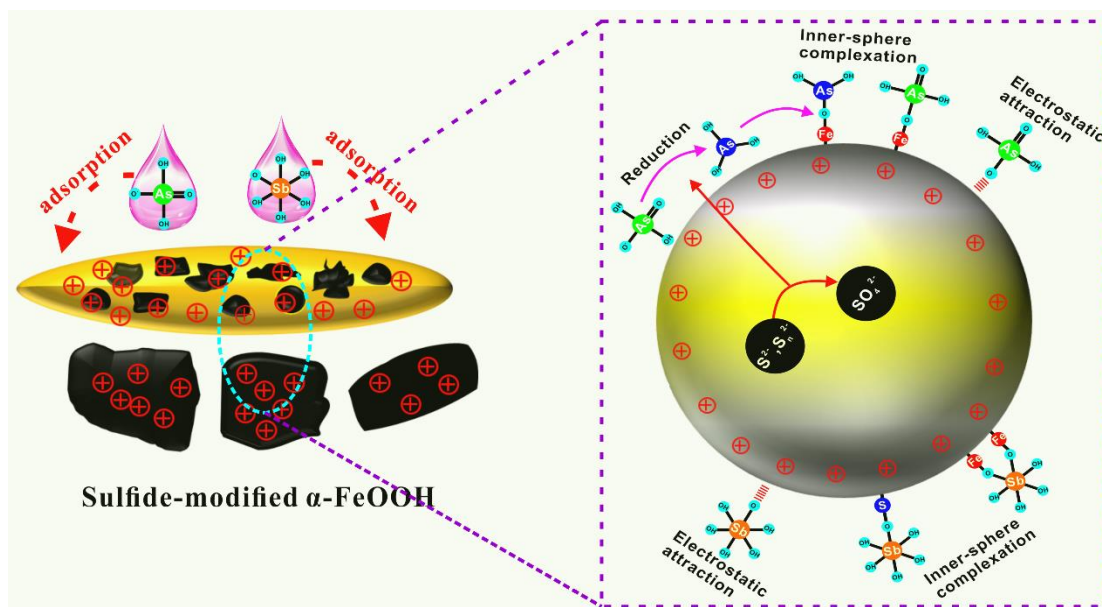
**Abstract**

Efficient elimination of As(V) and Sb(V) from wastewater streams has long been a major challenge. Herein, sulfide-modified α-FeOOH adsorbent was fabricated via a simple sulfidation reaction for removing As(V) and Sb(V) from aqueous media. Compared with the pristine α-FeOOH, sulfide-modified α-FeOOH increased the adsorption of As(V) from 153.8 to 384.6 mg/g, and Sb(V) adsorption from 277.8 to 1111.1 mg/g. The enhanced adsorption of both As(V) and Sb(V) was maintained at the pH range from 2 to 11, and was not interfered by various coexisting anions such as $Cl^-$, $SO_4^{2-}$, $NO_3^-$, $SiO_3^{2-}$ and $PO_4^{3-}$. The adsorption affinity increased from 0.0047 to 0.0915 and 0.0053 to 0.4091 for As(V) and Sb(V), respectively. X-ray photoelectron spectroscopic investigation demonstrated a reductive conversion of As(V) to As(III) during the adsorption process with sulfide-modified α-FeOOH, but with no obvious variation of Sb(V) speciation. While the removal mechanism for As(V) was reduction followed by adsorption via hydroxyl groups, mainly surface complexation was involved in the removal of Sb(V). This study presented a simple strategy to enhance the adsorption capacity and adsorption affinity of α-FeOOH toward As(V)/Sb(V) via sulfide-modification.

**Keywords:** Adsorption affinity and capacity; Arsenic and antimony; Iron-based adsorbents; Metalloid speciation; Sulfide-modification; Wastewater treatment.

**Capsule:** Sulfide-modified α-FeOOH remediates both low and high arsenic/antimony

49     levels under varying pH and competitive anions – conditions common in wastewater.

50

**1. Introduction**

Severe pollution of arsenic (As) and antimony (Sb) in natural water has triggered ever-increasing worldwide concerns, owing to the grave threats of these elements to human health (Fendorf et al., 2010; Herath et al., 2017). Anthropogenic factors such as mining activities, coal burning, and industrial consumption of As- and Sb-containing materials are primarily responsible for the build-up of these elements in the soil and water systems (Fawcett et al., 2015; Wei et al., 2015). Long term exposure to elevated concentrations of As and Sb could damage tissues and organs in human, and may even lead to cancer (Zhang et al., 2020; Smith et al., 2018; Winship, 1987; Herath et al., 2017). In view of the significant menaces of As and Sb on human health, the maximum contamination levels (MCLs) in drinking water for As (10.0 μg/L) and Sb (5.0 μg/L) were regulated by the US Environmental Protection Agency (USEPA) and World Health Organization (WHO) (Yamamura et al., 2003; Wang et al., 2018b). Furthermore, As and Sb exhibit homologous chemical and toxicological features, and these two metals often co-exist in many contaminated sites (Ungureanu et al., 2015). Therefore, effective technologies are needed to eliminate As and Sb from contaminated water and soil.

Various methods have been utilized to scavenge As and Sb from wastewater, such as adsorption (Lin et al., 2019; Mukhopadhyay et al., 2019), electrocoagulation (Cao et al., 2017), membrane filtration (Bolisetty et al., 2017), coprecipitation (Yuan et al., 2019), and ion exchange (Lee et al., 2017). Adsorption was considered as the most widely adopted methods by the virtue of its high removal efficiency, easy operation,

73 and low cost. Numerous adsorbents have been employed to purge As and Sb in

74 contaminated water, including biochar (Niazi et al., 2018; Han et al., 2017), metal

75 oxides (Qiu et al., 2019; Wang et al., 2016), metal-organic frameworks (Liu et al.,

76 2018a), graphene oxide (Yang et al., 2015) and clay minerals (Mukhopadhyay et al.,

77 2017; 2019; Sarkar et al., 2013). Among the adsorbents, iron materials were considered

78 to be the most potential ones for As and Sb removal, owing to merits such as abundant

79 source, low cost, excellent reactivity, and environmental friendliness (Wei et al., 2019;

80 Zhang et al., 2017; Wang et al., 2018a). Nevertheless, the adsorption affinity and

81 capacity of iron oxy-hydroxides toward As and Sb could be relatively weak, which

82 might hinder the practical utilization of iron-based adsorbents for wastewater treatment.

83     When seeking or designing materials with high adsorption affinity and capacity

84 toward As and Sb, it is worth to pay attention that the toxicity of As and Sb to human

85 mainly owes to the puissant affinity between As/Sb and sulfhydryl groups in proteins

86 (Lin et al., 1999; Ning and Xiao, 2007). Furthermore, As and Sb are both sulfophilic

87 elements, mainly exist in the form of sulfide deposits in the nature. The dominant As

88 minerals are orpiment ($As_2S_3$), realgar ($As_4S_4$) and arsenopyrite (FeAsS) (Bowell et al.,

89 2014). Similarly, antimony trisulfide ($Sb_2S_3$) is the main sulfide mineral in the case of

90 Sb (Okkenhaug et al., 2011). In marine systems, aquifers, and river and lake sediments,

91 sulfate reducing bacteria mediate sulfate reduction resulting in the formation of soluble

92 sulfide, and it further reacts with As or Sb to form orpiment ($As_2S_3$), realgar ($As_4S_4$),

93 arsenopyrite (FeAsS), or stibnite ($Sb_2S_3$) (Pope et al., 2004; O'Day et al., 2004).

94 Accordingly, sulfur act an vital role on the cycling of As and Sb in the environment,

95 and from this perspective, designing sulfur-based materials could be a promising

96 strategy for enhanced removal of As and Sb from aqueous media.

97    Goethite ($\alpha$-FeOOH) is a ubiquitous iron oxyhydroxide found in sediments, rocks

98 and soils, and thermodynamically highly stable in nature (Oganessian et al., 2017). $\alpha$-

99 FeOOH has previously been utilized for scavenging As and Sb from contaminated

100 water (Zhang et al., 2017; Xi et al., 2013). In anoxic conditions of a subsurface

101 environment, S(-II) originating from microbial sulfate reduction could transform iron

102 oxyhydroxides into iron sulfide or polysulfide. Inspired from the natural iron

103 oxyhydroxide transformation process induced by S(-II), we put forward a novel sulfide-

104 modification of $\alpha$-FeOOH for enhancing the adsorption of As(V) and Sb(V) from

105 wastewater. To the best of our knowledge, only limited number of studies have focused

106 on sulfide-modified $\alpha$-FeOOH as the adsorbent for scavenging As(V), and no study

107 investigated the comparative removal of As(V) and Sb(V) from polluted water (Hao et

108 al., 2018).

109    The objectives of this work are to: (1) fabricate a collection of sulfide-modified $\alpha$-

110 FeOOH materials with various S/Fe ratios, (2) investigate the structural and

111 morphological information of sulfide-modified $\alpha$-FeOOH via scanning electron

112 microscopy (SEM), Fourier transform infrared spectroscopy (FTIR), X-ray diffraction

113 (XRD), and X-ray photoelectron spectroscopy (XPS), (3) explore the adsorption

114 features of As(V) and Sb(V) on sulfide-modified $\alpha$-FeOOH via performing pH, kinetics,

115 isotherm, coexisting anions experiments, and (4) propose the possible mechanisms of

116 As(V)/Sb(V) adsorption on the sulfide-modified $\alpha$-FeOOH.

## 2. Materials and methods

2.1 Reagents

Sodium hydroxide (NaOH), hydrochloric acid (HCl), iron(III) nitrate nonahydrate ($Fe(NO_3)_3 \cdot 9H_2O$), sodium arsenate ($Na_3AsO_4 \cdot 12H_2O$), potassium antimonate hydrated ($KSb(OH)_6$), sodium hyposulfite ($Na_2S_2O_4$), sodium chloride (NaCl), sodium sulphate ($Na_2SO_4$), sodium nitrate ($NaNO_3$), sodium silicate ($Na_2SiO_3$), and sodium dihydrogen phosphate ($NaH_2PO_4$) were all of analytical grade, and obtained from Sinopharm Chemical Reagent Co. Ltd, China. $KSb(OH)_6$ and $Na_3AsO_4 \cdot 12H_2O$ were dissolved in ultrapure water to prepare the Sb(V) and As(V) stock solutions, respectively. The As(V) and Sb(V) working solutions were obtained through diluting the stock solutions. In all the batch experiments, a background electrolyte concentration was maintained by 0.1 M $KNO_3$.

2.2 Synthesis of α-FeOOH

A hydrothermal method was employed to synthesize α-FeOOH (Padhi and Parida, 2014). Briefly, certain amount of $Fe(NO_3)_3 \cdot 9H_2O$ was dissolved in ultrapure water under vigorous stirring, subsequently the solution pH was adjusted to 12 via NaOH addition, and further stirred for 30 min. Then, the reddish-brown mixture was transferred into a 100 mL Teflon-lined autoclave for hydrothermal reaction for 24 h at 180℃. After reaction, the autoclave was cooled down, and the obtained yellow product was repeatedly washed with ultrapure water until the supernatant pH was neutral. Then,

139   the product was separated by centrifugation (6000 rpm for 5 min), and dried at 60℃

140   for 48 h.

141

142   2.3 Synthesis of sulfide-modified α-FeOOH

143      The sulfide-modified α-FeOOH was fabricated by using dithionite as the

144   sulfidation reagent (Kim et al., 2011). Typically, certain amount of α-FeOOH was

145   suspended in de-oxygenated ultrapure water (in 250 mL three-neck flask), and

146   ultrasonicated for 30 min. Then, 1 mol/L $Na_2S_2O_4$ solution was freshly prepared by

147   dissolving $Na_2S_2O_4$ in de-oxygenated ultrapure water. Under nitrogen atmosphere,

148   certain volume of fresh $Na_2S_2O_4$ solution with different S/Fe ratios (S/Fe= 0.1, 0.3, 0.5,

149   0.8, 1.0) were drop-wise added to the α-FeOOH suspension, sealed the bottle, and

150   agitated for another 48 h. The obtained precipitate was washed by de-oxygenated

151   ultrapure water for several times, and separated by centrifugation. The product was

152   finally dried in a vacuum oven. The step-wise synthesis procedure is shown

153   schematically in Supplementary Information (SI; Fig. S1).

154

155   2.4 Adsorbent characterization

156      The crystal composition of sulfide-modified α-FeOOH was characterized by XRD

157   (D8 Advance, Bruker, Germany) performed with Cu Kα radiation (λ = 1.5418 Å) at the

158   2θ range of 10° to 80°. FTIR spectra of the adsorbents were collected by an IR Prestige-

159   21 spectrometer (Shimadzu, Japan) at the wavelength scope of $4000 - 400$ $cm^{-1}$ via KBr

160   pellet method. To investigate the surface chemical composition and elemental valence

states in the adsorbents, XPS investigation was conducted on a PHI Quantera II ESCA

system (Ulvac-Phi, Japan) with a monochromatic Al Kα radiation at 1486.8 eV. The

binding energy of the data was calibrated to the C1s peak at 284.8 eV. The surface

morphology of the adsorbents was observed by SEM associated with energy dispersion

spectrometer (EDS) (Quanta 250FEG, FEI, USA). Certain amount of adsorbent was

dispersed in water at pH range of 2 to 11, and the solution pH was preserved at the

desired value and adjusted every 6 h. Then, the zeta potential values of the adsorbents

were measured by a zetasizer (ZetaPALS, Brookhaven, USA).

2.5 Batch experiments

Batch adsorption experiments were performed to investigate the effect of contact

time, initial adsorbate concentration, initial pH and coexisting anions on the adsorption

behavior of As(V) and Sb(V) by sulfide-modified α-FeOOH. A 100 mL conical bottle

containing 50 mL As(V) or Sb(V) solution was adopted for all the batch adsorption

experiments implemented in duplicate. The fabricated adsorbents were added at a

dosage of 0.5 g/L, and a background ionic strength was maintained by 0.1 M KNO₃.

The conical bottles were sealed, and shaken on an oscillator at 200 rpm for 24 h at 25℃.

After adsorption, supernatants were filtered through 0.22 μm membrane filter for

determining the residual aqueous concentration of As(V) or Sb(V). Furthermore,

adsorbents after adsorption were collected by centrifugation, washed and dried at

vacuum, and used for the characterization studies. The adsorption capacity (mg/g) of

As(V) and Sb(V) on the adsorbents was obtained using Eq. 1:

$$q_e = \frac{(C_0 - C_e)V}{m} \tag{1}$$

where, $q_e$ (mg/g) represents the equilibrium adsorption capacity; $C_0$ and $C_e$ (mg/L)

represent the supernatant concentrations of adsorbate at the initial and equilibrium times,

respectively; V (L) is the adsorbate volume; and m (g) is the mass of the adsorbent.

To examine the influence of pH on adsorption, the solution pH was varied from 2

to 11 adjusted via adding 1 M $HNO_3$ or NaOH solutions. The solution pH was preserved

at the desired value and adjusted every 6 h to avoid any change of the solution pH.

Apart from the initial pH effect, a constant pH value of 3 was adopted for all other

experiments. To explore the time-dependent adsorption behavior, adsorbent (0.5 g/L)

was transferred to an initial As(V) or Sb(V) concentration of 300 mg/L or 500 mg/L (50

mL), respectively. Aliquots of suspension was sampled at different time intervals to

determine the residual As(V) and Sb(V) concentration. Adsorption isotherm

investigations were performed at the initial concentration varying from 50 to 500 mg/L.

Effects of commonly coexisting anions in wastewater on adsorption performance of

As(V) and Sb(V) were explored by conducting the adsorption tests with 200 mg As or

Sb/L in 500 mg/L sodium salt solutions of various anions (NaCl, $Na_2SO_4$, $NaNO_3$,

$Na_2SiO_3$, $NaH_2PO_4$).

2.6 Analysis of As and Sb

Inductively coupled plasma-optical emission spectrometer (ICP-OES) (7000DV,

Perkin Elmer, USA) was used to measure the concentrations of As and Sb in the aliquots.

Samples were diluted where needed, acidified with 1% $HNO_3$, and analyzed within 48

h. The displayed data in this study were the average values of duplicate experiments.

205

**3. Results and discussion**

3.1 Characterization of sulfide-modified α-FeOOH

The pure α-FeOOH exhibited a uniform acicular morphology (Fig. 1a). The sulfide-modification significantly changed the appearance of α-FeOOH. When the S/Fe mole ratio increased from 0 to 0.3, the sulfide-modification of α-FeOOH caused a variation of particle length (Fig. 1a-c), but the sulfide-modified α-FeOOH still kept the acicular morphology (Fig. 1b and c). When controlling the S/Fe mole ratio from 0.5 to 1.0, the acicular morphology was significantly destroyed, which was followed by the formation of larger aggregates (Fig. 1d-f). Due to the increase of S/Fe mole ratio, the acicular shape became shorter, and even was damaged to form large sized rough and irregular particles.

The functional groups of sulfide-modified α-FeOOH with different S/Fe mole ratios was obtained by FTIR (Fig. 2a). The band at 3111 cm$^{-1}$ represented the stretching vibration of O-H (Liu et al., 2017), which reflected the non-stoichiometric hydroxyl groups of α-FeOOH. The intensity of O-H band was weakened along with the increasing S/Fe mole ratio, revealing a reduction of hydroxyl groups on sulfide-modified α-FeOOH. This might be attributed to the partial transformation of α-FeOOH to sulfur-bearing iron minerals. The bands at 790 and 890 cm$^{-1}$ were ascribed to the Fe-O-H bending vibrations of α-FeOOH (Rahimi et al., 2015; Liu et al., 2018b). The Fe-O-H bands also exhibited an attenuating trend with the increase of S/Fe mole ratio. Meanwhile, the band at 609 cm$^{-1}$ was attributed to the Fe-O stretching of α-FeOOH

227 (Wei et al., 2017). After sulfide-modification, a new band located at 1134 cm$^{-1}$ was

228 observed, which could relate to the superficial oxidation of $FeS_2$ (Jiang et al., 2015). No

229 significant stretching frequency concerning FeS was detected (Gong et al., 2014).

230     The crystal phases of the sulfide-modified α-FeOOH were identified by XRD (Fig.

231 2b). The pure α-FeOOH exhibited a space group symmetry of Pbnm (Z = 4) with the

232 lattice parameters of $a$ = 4.55979 Å, $b$ = 9.951 Å, and $c$ = 3.0178 Å (Yang et al., 2006).

233 The diffraction peaks of pure α-FeOOH (JCPDS No. 29-0713) at 2θ values 17.80º,

234 21.22º, 26.32º, 33.24º, 34.70º, 36.65º, 41.19º, 53.24º and 59.02º were indexed as the

235 Bragg reflections of (020), (110), (120), (130), (021), (111), (140), (221), and (151)

236 crystal planes, respectively. The diffraction peaks of the main crystal planes of α-

237 FeOOH were still detected after sulfidation (Fig. 2b), indicating that the sulfide-

238 modification did not destroy the original crystal structure of α-FeOOH. However, the

239 intensity of the diffraction peaks was abated with the increase of S/Fe mole ratio, which

240 was similar with other modified α-FeOOH (Liu et al., 2018c). When the S/Fe ratio was

241 higher than 0.3, a new reflection located at 2θ = 32.7° could be indexed to plane (2 1 1)

242 of FeS (JCPDS No. 76-0964).

243     XPS spectra were collected to further investigate the surface composition of the

244 sulfide-modified α-FeOOH materials. The two main peaks of Fe 2p spectrum at the

245 binding energy (BE) of ～725.1 eV and ～711.1 eV (Fig. 3a-d) represented Fe $2p_{1/2}$

246 and Fe $2p_{3/2}$, respectively (Zhang et al., 2019). The fitted Fe 2p spectra in Fig. 3a and b

247 showed the features of Fe(III). With further increase of the S/Fe ratio, the binding

248 energies at 710.1 eV, 724.3 eV, and 710.2 eV (Fig. 3c and d) could be assigned to Fe(II)

species existing on the surface (Tang et al., 2017; Wan et al., 2014). The observed signals of Fe(II) species indicated the reduction transformation of Fe(III) to Fe(II) in $\alpha$-FeOOH by sulfide (Wan et al., 2014). Meanwhile, the reduced concentration of $O^{2-}$ in O1s spectra (Fig. 3e-h) could be assigned to the partial replacement of Fe-O groups by Fe(II)-S groups. The abundance of sulfur species was enhanced with the gradual rise of S/Fe molar ratio, which was previously observed for sulfide-modified zero valent iron (S-ZVI) (Xu et al., 2019). Additionally, disulfide ($S_2^{2-}$) (BE $\sim$ 66.6 eV), polysulfide ($S_n^{2-}$) (BE $\sim$ 167.7 and 166.6 eV), and sulfite ($SO_3^{2-}$) (BE $\sim$ 169.4 and 168.2 eV) species on the sulfide-modified $\alpha$-FeOOH surface (Fig. 3i-k) were confirmed (Mangayayam et al., 2019). Therefore, the XPS results suggested that sulfide was biding with Fe(II) which originated from the reduction of Fe(III) in $\alpha$-FeOOH. The sulfur species of $S_2^{2-}$, $S_n^{2-}$ and $SO_3^{2-}$ were generated from the hydrolysis of $Na_2S_2O_4$ (Eq. 2-6).

$$2S_2O_4^{2-} + H_2O \rightarrow S_2O_3^{2-} + 2SO_3^{2-} + 2H^+ \qquad (2)$$

$$S_2O_4^{2-} + S_2O_3^{2-} + 2H_2O + H^+ \rightarrow 3HSO_3^- + H_2S \qquad (3)$$

$$H_2S \rightarrow S^{2-} + 2H^+ \qquad (4)$$

$$S_2O_3^{2-} \rightarrow SO_3^{2-} + S \qquad (5)$$

$$S^{2-} + S + FeOOH \rightarrow FeS_2 + H_2O \qquad (6)$$
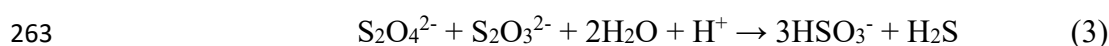
Surface charge of an adsorbent is a key property that influences the adsorption of metal(loid) ions through electrostatic attraction. An adsorbent with low point of zero charge ($pH_{pzc}$) favors the removal of cationic heavy metals (e.g., Cu, Cd, Pb, Ni). For oxyanions of heavy metal(loid)s such as As, Sb and Se, a high $pH_{pzc}$ would result in

271 greater adsorption via electrostatic attraction. The zeta potential values of α-FeOOH

272 and sulfide-modified α-FeOOH suspensions were determined at the pH range of 2 to 11

273 (Fig. 4). The pristine α-FeOOH exhibited a $pH_{pzc}$ of 6.69. The $pH_{pzc}$ value of sulfide-

274 modified α-FeOOH significantly increased from 6.69 to 7.40, 7.64, 10.29, 10.39 and

275 10.43 when the S/Fe ratio increased to 0.1, 0.3, 0.5, 0.8 and 1.0, respectively. Similar

276 phenomenon was found in other thiol-functionalized or sulfide modified iron materials

277 (Ma et al., 2018; Ji et al., 2019). A positively charged surface of sulfide-modified α-

278 FeOOH was exhibited at pH =10 when the S/Fe ratio was greater than 0.3 (Fig. 4).

279 Therefore, adsorbents with an increased positive surface charge were resulted following

280 the sulfide-modification, which was a merit of the sulfide-modified α-FeOOH favoring

281 the adsorption of metal(loids) like As(V) and Sb(V).

282

283 3.2 Effect of pH on adsorption

284     Metal(loid) adsorption by adsorbents might highly rely on the solution pH which

285 could affect the surface charge of the adsorbents, and the existing metal(loid) species

286 (Prabhu et al., 2019; Wang et al., 2016). The influence of pH on the removal of As(V)

287 and Sb(V) was tested in the pH range of 2.0 to 11.0. The adsorption capacities of sulfide-

288 modified α-FeOOH were higher than the pristine α-FeOOH in the entire pH range (2.0

289 to 11.0) (Fig. 5). The adsorption of As(V)/Sb(V) was pH dependent, and the adsorption

290 capacities gradually decreased with the increase of pH from 2.0 to 11.0. Similar

291 tendency was observed for oxyanion adsorption on Ce(III)–doped $Fe_3O_4$ (Qi et al.,

292 2017), La-doped magnetic biochar (Wang et al., 2018b), FeOOH nanoparticles (Zhang

293 et al., 2017), and Fe-Ti-Mn composite oxide (Zhang et al., 2019d). The gradual drop of

294 adsorption capacity with an increase of solution pH could be ascribed to the conversion

295 of surface charge from positive to negative values (Fig. 4) together with the varied

296 inorganic As(V)/Sb(V) species (Fig. S2). The forms of As(V) likely were $H_2AsO_4^-$,

297 $HAsO_4^{2-}$ and $AsO_4^{3-}$ when pH varied from 2.0 to 11.0 (Fig. S2). The hydrolysis of

298 $H_3AsO_4$ and $Sb(OH)_5$ generated anionic species of the elements ($H_2AsO_4^-$, $HAsO_4^{2-}$,

299 $AsO_4^{3-}$ and $Sb(OH)_6^-$) with the increase of pH value. These anions might compete with

300 $OH^-$ ions for the adsorption sites at high solution pH (Liu et al., 2016a). Furthermore,

301 the Coulombic repulsion between As(V) or Sb(V) oxyanions and the declining surface

302 positive charge of sulfide-modified α-FeOOH could be accountable for the decreased

303 adsorption of As(V)/Sb(V) at high solution pH.

304

305 3.3 Adsorption kinetics

306 The influence of reaction time on the adsorption behavior of As(V) and Sb(V) by

307 the sulfide-modified α-FeOOH was illustrated (Fig. S3). Adsorption reactions of

308 As(V) and Sb(V) by the sulfide-modified α-FeOOH was rapid within the first 100

309 min, and more than 80% of the equilibrium adsorption was achieved during this time

310 (Fig. S3a and d). Subsequently, a slower adsorption rate occurred until the equilibrium

311 was reached. This kind of adsorption pattern occurred mainly due to the abundance of

312 adsorption sites at the beginning of the reaction, and as time went on, the active sites

313 were occupied by oxyanions, which then brought about the low adsorption rate

314 toward the end of the reaction. To further investigate the adsorption kinetics process,

the pseudo-first order and pseudo-second order were adopted to fit the experiment

data. A higher coefficient of determination ($R^2$) (Table 1; Fig. S3b, c, e and f)

indicated that the pseudo-second order model adequately described the As(V)/Sb(V)

adsorption behaviors on the adsorbent. It was inferred that the adsorption of As(V)

and Sb(V) on sulfide-modified α-FeOOH was controlled by chemical reactions

(Zhang et al., 2013). With an increase of the S/Fe ratio in the adsorbents, the

equilibrium adsorption capacity toward As(V) and Sb(V) increased from 70.92 to

285.7 mg/g, and 131.6 to 1000 mg/g, respectively (Table 1). To investigate the effect

of the materials on solution pH, the adsorbents were dispersed in ultrapure water with

a solid/liquid ratio at 0.025 g/50 mL. After shaking for 24 h, the final pH was

determined. The pH values were 7.20, 6.91, 6.58, 6.03, 5.87 and 5.72 for materials

with S/Fe ratio of 0, 0.1, 0.3, 0.5, 0.8 and 1.0, respectively. The final pH values were

further checked at the end of kinetic experiments at initial pH = 3 and adsorbent

dosage = 0.5 g/L. The solution pH did not change notably (Table S1).

3.4 Adsorption isotherm

The As(V) and Sb(V) adsorption amounts of the sulfide-modified α-FeOOH were

estimated via isotherm studies (Fig. S4a and d). The Langmuir and Freundlich model

(SI Text) fitting results are shown in Table 2, and Fig. S4b, c, e and f. The Langmuir

model was more appropriate (with greater $R^2$ value) than the Freundlich model to

explain the As(V) and Sb(V) sorption properties on sulfide-modified α-FeOOH. It

could be inferred that a homogeneous adsorption occurred on the surface of the

337    adsorbents. Based on the model fitting results (Table 2), the calculated maximum

338    adsorption capacities ($q_{max}$) were 153.8 – 384.6 mg/g, and 277.8 – 1111.1 mg/g for

339    As(V) and Sb(V), respectively. The $q_{max}$ values thus endowed the sulfide-modified α-

340    FeOOH adsorbents with outstanding potentials for practical remediation of As(V) and

341    Sb(V) in contaminated water with notably better performance than previously

342    published adsorbents (Table S2). The significant enhancement of the adsorption

343    capacity on the sulfide-modified α-FeOOH might be owing to the strong affinity

344    between sulfur and As(V)/Sb(V). The enhancement for Sb(V) was more remarkable

345    than As(V), and the adsorption capacity of the sulfide-modified α-FeOOH at S/Fe=1.0

346    was 3.99 and 2.5 times higher for As(V) and Sb(V), respectively, than the pristine α-

347    FeOOH.

348        The $q_{max}$ and Langmuir constant b are two important parameters reflecting the

349    adsorption capacity and adsorption affinity, respectively. Large $q_{max}$ value is

350    beneficial for remediating high adsorbate concentration (e.g., industrial wastewater),

351    whereas large b value is important for low adsorbate concentration needing

352    remediation (e.g., groundwater and drinking water). At low adsorbate concentration, a

353    small $q_{max}$ value with large b value could gain higher $q_e$ than the situation of large $q_{max}$

354    and small b values (Cao et al., 2012). As presented in Table 2, the $q_{max}$ and b values

355    for As(V)/Sb(V) adsorption were increased with increasing S/Fe ratio in the

356    adsorbents. The enhancement of $q_{max}$ and b values for Sb(V) was more remarkable

357    than As(V). The overall results thus indicated that sulfide-modification could

358    dramatically increase the adsorption capacity and affinity of As(V) and Sb(V) on the

359 modified adsorbents, which is beneficial for the practical remediation of As(V) and

360 Sb(V) in polluted water at different contamination levels.

361

362 3.5 Effect of coexisting anions

363　　A great deal of anions can co-occur with As(V) or Sb(V) in wastewater

364 environment, which might interfere with the elimination of As(V) or Sb(V) by

365 adsorbents. The co-existing anions including $Cl^-$, $SO_4^{2-}$, $NO_3^-$, and $SiO_3^{2-}$ in this study

366 displayed a marginal influence on As(V)/Sb(V) adsorption by sulfide-modified α-

367 FeOOH (Fig. 6). However, $PO_4^{3-}$ exhibited a significant hindrance on As(V)/Sb(V)

368 removal, indicating that $PO_4^{3-}$ possessed a strong competition for active adsorption

369 sites on the surface of sulfide-modified α-FeOOH. The elements P, As and Sb belong

370 to the same VA group in the periodic table. The similar atomic structure and

371 hydrolysis behavior of $PO_4^{3-}$ and As(V) or Sb(V) (Zhang et al., 2019c) could cause the

372 strong competition during the adsorption process, thereby impacting the As(V)/Sb(V)

373 adsorption capacity of the adsorbent in the presence of $PO_4^{3-}$.

374

375 3.6 Adsorption mechanisms

376　　To reveal the role of sulfide-modification on As(V) or Sb(V) sorption by sulfide-

377 modified α-FeOOH, the surface chemical environments of the sulfide-modified α-

378 FeOOH before and after As(V)/Sb(V) adsorption were further studied by XPS. The

379 high resolution As3d spectra of As(V)-adsorbed α-FeOOH and sulfide-modification α-

380 FeOOH were shown in Fig. 7a. Compared to the As3d spectra of As(V)-adsorbed α-

381 FeOOH (BE $\sim$ 45.9 eV), a combined spectra showing both As(V) 3d and As(III) 3d

382 peaks was observed for As-adsorbed sulfide-modified α-FeOOH. Specifically, the BE

383 of 45.7 eV, 46.2 eV and 45.9 eV could be assigned to As(V), and 45.1 eV, 45.4 eV and

384 45.2 eV could be assigned to As(III) for the S/Fe ratio of 0.3, 0.5, 1.0, respectively (Wu

385 et al., 2018; Penke et al., 2019; Zhou et al., 2020). The sulfide-modified α-FeOOH thus

386 exhibited a reductive transformation of As(V) to As(III) with the raise of S/Fe ratios,

387 where the percentage of As(III) was 40.46, 55.11, and 70.70% of the total As for the

388 S/Fe ratio of 0.3, 0.5 and 1.0, respectively. The reduction of As(V) by sulfide-modified

389 α-FeOOH could be attributed to the introduced sulfur species ($S_2^{2-}$, $S_n^{2-}$ and $SO_3^{2-}$).

390 Therefore, As(V) was partially reduced to As(III), which likely contributed to the

391 enhanced removal of As(V) by the sulfide-modified α-FeOOH. This phenomenon was

392 also observed in the case of As(V) removal using FeS adsorbent (Liu et al., 2016b).

393 However, the BE of Sb3d spectra (Fig. 7b) after Sb(V) adsorption on α-FeOOH and

394 sulfide-modified α-FeOOH showed no significant variation. Specifically, the BE of

395 Sb3d were 540.0, 540.2, 540.4, and 540.2 eV for different S/Fe ratios, assigning all the

396 peaks to Sb(V) only (He et al., 2019; Liu et al., 2019). Therefore, no reduction of Sb(V)

397 occurred on the surface of sulfide-modified α-FeOOH. Similar phenomenon was

398 reported during the removal of Sb(V) by $FeS_2$/α-$Fe_2O_3$ (He et al., 2019). The sulfide-

399 modified α-FeOOH in this study exhibited chemical constituents of $FeS_2$/α-FeOOH (as

400 depicted by the XPS and FTIR results), which is similar to previously reported $FeS_2$/α-

401 $Fe_2O_3$ adsorbents (He et al., 2019). It could be speculated that the ≡Fe-OH and ≡S-

402 H were both responsible for the removal of Sb(V) by sulfide-modified α-FeOOH.

403    The morphology of sulfide-modified α-FeOOH after As(V) and Sb(V) adsorption

404    are shown in Fig. S5-S8. When the S/Fe ratio was less than 0.3, there was no obvious

405    variation in the needle-like particles after reacting with As(V) (Fig. S5b, e and h) and

406    Sb(V) (Fig. S7b, e and h), as compared with original adsorbents (Fig. 1). However,

407    when the S/Fe ratio was higher than 0.3, the morphology of the adsorbents was

408    dramatically altered after interacting with As(V) (Fig. S6) and Sb(V) (Fig. S8), and

409    irregular small particles were formed. The peaks of As or Sb were observed in

410    corresponding EDS spectra after removed by sulfide-modified α-FeOOH (Fig. S5-S8).

411    Furthermore, the intensity of As and Sb peaks in the respective EDS spectrum became

412    stronger along the raise of S/Fe ratio, indicating that the sulfide-modification improved

413    the adsorption capacity of α-FeOOH toward As(V) and Sb(V).

414    To explain the role of Fe and S on the elimination of As(V)/Sb(V) by sulfide-

415    modified α-FeOOH, variations of Fe and S species after the adsorption process were

416    also studied by XPS. The Fe2p and S2p spectra of sulfide-modified α-FeOOH (S/Fe=1.0)

417    pre-and post-adsorption of As(V) and Sb(V) are shown in Fig. S9. The peaks at 710.0

418    and 724.2 eV were assigned to $Fe^{2+}$ signals (Wan et al., 2014), and these two peaks

419    shifted to 711.3 and 725.3 eV, and 710.8 and 724.8 eV after the sorption of As(V) and

420    Sb(V), respectively (Fig. S9a), implying that $Fe^{2+}$ was partially oxidized to $Fe^{3+}$.

421    Therefore, the ≡Fe-OH functional groups likely contributed to the sorption of As(V)

422    and Sb(V). The S2p spectra also exhibited a significant variation after As(V) and Sb(V)

423    adsorption (Fig. S9b). The S species in the original sulfide-modified α-FeOOH were

424    $S_2^{2-}$, $S_n^{2-}$ and $SO_3^{2-}$, but the $S^{2-}$ species disappeared after the adsorption, leaving behind

425 only $SO_3^{2-}$ and $S_n^{2-}$. These results indicated that S species were oxidized, and

426 participated in the reduction of As(V). The ≡S-H functional groups were likely involved

427 in the removal of Sb(V) (He et al., 2019).

428    Based on the discussion above, the conceived adsorption mechanisms between

429 sulfide-modified α-FeOOH and As(V)/Sb(V) could be summarized as the following:

430    (1) The adsorption kinetics for sulfide-modified α-FeOOH toward As(V)/Sb(V)

431 were well expressed by the pseudo second order, demonstrating that the adsorption

432 process of As(V) and Sb(V) on sulfide-modified α-FeOOH was controlled by a

433 chemical reaction mechanism.

434    (2) The XPS results suggested that the abundant S species on sulfide-modified α-

435 FeOOH converted As(V) to As(III); the ≡S-H functional groups were involved in the

436 adsorption of Sb(V).

437    (3) The pH effect on adsorption indicated that electrostatic attraction also

438 contributed to the As(V)/Sb(V) removal process. The sulfide-modified α-FeOOH held

439 more positive surface charges than α-FeOOH, which was in favor of As(V)/Sb(V)

440 removal. The sulfide-modified α-FeOOH exhibited the crystal phase of α-FeOOH, and

441 contained abundant surface hydroxyl groups (as confirmed by XPS and FTIR).

442 Therefore, the As(V/III) and Sb(V) were adsorbed through surface complexation

443 reactions too via the ≡Fe-OH groups.

444

445 **4. Conclusions**

446    In this work, a novel sulfide-modified α-FeOOH was synthesized, and utilized

447  for As(V) and Sb(V) removal from aqueous solutions. The sulfide-modification

448  exhibited significant effect on the morphology, crystal phases, surface composition,

449  and surface charge of the α-FeOOH, consequently influenced the As(V)/Sb(V)

450  adsorption performance. The sulfide-modified α-FeOOH increased the adsorption

451  capacities of As(V) and Sb(V), but it was more notable for Sb(V). The adsorption

452  affinity of sulfide-modified α-FeOOH toward As(V) and Sb(V) were also increased

453  with increasing S/Fe ratio in the adsorbents. The kinetic and isotherm investigations

454  implied that chemisorption and monolayer adsorption controlled the removal of As(V)

455  and Sb(V) by the sulfide-modified α-FeOOH. The sulfide-modified α-FeOOH

456  possessed a reducibility effect toward As(V), but not toward Sb(V). Overall, this

457  study put forward a strategy to increase the adsorption affinity and capacity of As(V)

458  and Sb(V) on α-FeOOH via sulfide modification. The sulfide-modified α-FeOOH thus

459  exhibited promising implications for the remediation of As(V) and Sb(V) in aqueous

460  media containing both high and low adsorbate concentrations.

461

467

468  **Declaration of interest**

469    The authors declare no competing financial interests for this study.

470

471    **References**

472    Bolisetty, S., Reinhold, N., Zeder, C., Orozco, M.N., Mezzenga, R., 2017. Efficient

473        purification of arsenic-contaminated water using amyloid–carbon hybrid

474        membranes. Chem. Commun. 53, 5714-5717.

475    Bowell, R.J., Alpers, C.N., Jamieson, H.E., Nordstrom, D.K., Majzlan, J., 2014. The

476        environmental geochemistry of arsenic—an overview. Rev. Mineral. Geochem.

477        79, 1-16.

478    Cao, D., Zeng, H., Yang, B., Zhao, X., 2017. Mn assisted electrochemical generation

479        of two-dimensional Fe-Mn layered double hydroxides for efficient Sb(V)

480        removal. J. Hazard. Mater. 336, 33-40.

481    Cao, Q., Huang, F., Zhuang, Z., Lin, Z., 2012. A study of the potential application of

482        nano-$Mg(OH)_2$ in adsorbing low concentrations of uranyl tricarbonate from

483        water. Nanoscale 4, 2423-2430.

484    Fendorf, S., Michael, H.A., Geen, A., 2010. Spatial and temporal variations of

485        groundwater arsenic in South and Southeast Asia. Science 328, 1123-1127.

486    Fawcett, S.E., Jamieson, H.E., Nordstrom, D.K., McCleskey, R.B., 2015. Arsenic and

487        antimony geochemistry of mine wastes, associated waters and sediments at the

488        Giant Mine, Yellowknife, Northwest Territories, Canada. Appl. Geochem. 62, 3-

489        17.

490    Gong, Y., Liu, Y., Xiong, Z., Zhao, D., 2014. Immobilization of mercury by

491      carboxymethyl cellulose stabilized iron sulfide nanoparticles: reaction

492      mechanisms and effects of stabilizer and water chemistry. Environ. Sci. Technol.

493      48, 3986-3994.

494    Han, L., Sun, H., Ro, K.S., Sun, K., Libra, J.A., Xing, B., 2017. Removal of

495      antimony(III) and cadmium(II) from aqueous solution using animal manure-

496      derived hydrochars and pyrochars. Bioresour. Technol. 234, 77-85.

497    Hao, L., Liu, M., Wang, N., Li, G., 2018. A critical review on arsenic removal from

498      water using iron-based adsorbents. RSC Adv. 8, 39545-39560.

499    He, X., Min, X., Peng, T., Ke, Y., Zhao, F., Wang, Y., Sillanpää, M. (2019). Highly

500      Efficient Antimonate Removal from Water by Pyrite/Hematite Bi-Mineral:

501      Performance and Mechanism Studies. J. Chem. Eng. Data 64(12), 5910-5919.

502    Herath, I., Vithanage, M., Bundschuh, J., 2017. Antimony as a global dilemma:

503      geochemistry, mobility, fate and transport. Environ. Pollut. 223, 545-559.

504    Ji, J., Chen, G., Zhao, J., 2019. Preparation and characterization of amino/thiol

505      bifunctionalized magnetic nanoadsorbent and its application in rapid removal of

506      Pb(II) from aqueous system. J. Hazard. Mater. 368, 255-263.

507    Jiang, F., Peckler, L.T., Muscat, A.J., 2015. Phase pure pyrite $FeS_2$ nanocubes

508      synthesized using oleylamine as ligand, solvent, and reductant. Cryst. Growth

509      Des. 15, 3565-3572.

510    Kim, E.J., Kim, J.H., Azad, A.M., Chang, Y.S., 2011. Facile synthesis and

511      characterization of Fe/FeS nanoparticles for environmental applications. ACS

512      Appl. Mater. Interfaces 3, 1457-1462.

Lee, C.G., Alvarez, P.J.J., Nam, A., Park, S.J., Do, T., Choi, U.S., Lee, S.H., 2017. Arsenic(V) removal using an amine-doped acrylic ion exchange fiber: kinetic, equilibrium, and regeneration studies, J. Hazard. Mater. 325, 223-229.

Lin, L., Zhang, G., Liu, X., Khan, Z. H., Qiu, W., Song, Z. (2019). Synthesis and adsorption of Fe-Mn-La-impregnated biochar composite as an adsorbent for As(III) removal from aqueous solutions. Environ. Pollut. 247, 128-135.

Lin, S., Cullen, W.R., Thomas, D.J., 1999. Methylarsenicals and arsinothiols are potent inhibitors of mouse liver thioredoxin reductase. Chem. Res. Toxicol. 12, 924-930.

Liu, B., Jian, M., Wang, H., Zhang, G., Liu, R., Zhang, X., Qu, J., 2018a. Comparing adsorption of arsenic and antimony from single-solute and bi-solute aqueous systems onto ZIF-8. Colloids Surf. A Physicochem. Eng. Asp. 538, 164-172.

Liu, H., Lu, X., Li, M., Zhang, L., Pan, C., Zhang, R., Li, J., Xiang, W., 2018b. Structural incorporation of manganese into goethite and its enhancement of Pb(II) adsorption. Environ. Sci. Technol. 52, 4719-4727.

Liu, R., Liu, J.F., Zhang, L.Q., Sun, J.F., Jiang, G.B., 2016a. Low temperature synthesized ultrathin $\gamma$-Fe$_2$O$_3$ nanosheets show similar adsorption behaviour for As(III) and As(V). J. Mater. Chem. A 4, 7606-7614.

Liu, R., Yang, Z., He, Z., Wu, L., Hu, C., Wu, W., Qu, J., 2016b. Treatment of strongly acidic wastewater with high arsenic concentrations by ferrous sulfide (FeS): Inhibitive effects of S(0)-enriched surfaces. Chem. Eng. J. 304, 986-992.

Liu, Y., Liu, X., Zhao, Y., Dionysiou, D.D., 2017. Aligned $\alpha$-FeOOH nanorods

anchored on a graphene oxide-carbon nanotubes aerogel can serve as an effective

Fenton-like oxidation catalyst. Appl. Catal., B 213, 74-86.

Liu, Y., Wu, P., Liu, F., Li, F., An, X., Liu, J., Wang, Z., Shen, C., Sand, W. (2019).

Electroactive modified carbon nanotube filter for simultaneous detoxification

and sequestration of Sb(III). Environ. Sci. Technol. 53(3), 1527-1535.

Ma, R., Yin, L., Li, L., Zhang, S., Wen, T., Zhang, C., Wang, X., Chen, Z., Hayat, T.,

Wang, X., 2018. Comparative Investigation of $Fe_2O_3$ and $Fe_{1-x}S$ Nanostructures

for Uranium Decontamination. ACS Appl. Nano Mater. 1, 5543-5552.

Mangayayam, M., Dideriksen, K., Ceccato, M., Tobler, D.J., 2019. The Structure of

Sulfidized Zero-Valent Iron by One-Pot Synthesis: Impact on Contaminant

Selectivity and Long-Term Performance, Environ. Sci. Technol. 53, 4389-4396.

Mukhopadhyay, R., Manjaiah, K.M., Datta, S.C., Sarkar, B., 2019. Comparison of

properties and aquatic arsenic removal potentials of organically modified

smectite adsorbents. J. Hazard. Mater. 377, 124-131.

Mukhopadhyay, R., Manjaiah, K.M., Datta, S.C., Yadav, R.K., Sarkar, B., 2017.

Inorganically modified clay minerals: Preparation, characterization, and arsenic

adsorption in contaminated water and soil. Appl. Clay Sci. 147, 1-10.

Niazi, N.K., Bibi, I., Shahid, M., OK, Y.S., Burton, E.D., Wang, H., Shaheen, S.M.,

Rinklebe, J., Lüttge, A., 2018. Arsenic removal by perilla leaf biochar in aqueous

solutions and groundwater: an integrated spectroscopic and microscopic

examination. Environ. Pollut. 232, 31-41.

Ning, Z., Xiao, T., 2007. Supergene geochemical behavior and environmental risk of

557    antimony. Earth Environ. 35, 176-182.

558    O'Day, P.A., Vlassopoulos, D., Root, R., Rivera, N., 2004. The influence of sulfur and

559    iron on dissolved arsenic concentrations in the shallow subsurface under

560    changing redox conditions. Proc. Natl. Acad. Sci. U. S. A. 101, 13703-13708.

561    Oganessian, N.V.T., Guda, A.A., Sakhnenko, V.P., 2017. Linear magnetoelectric effect

562    in göthite, $\alpha$-FeOOH. Sci. Rep. 7, 16410.

563    Okkenhaug, G., Zhu, Y.G., Luo, L., Lei, M., Li, X., Mulder, J., 2011. Distribution,

564    speciation and availability of antimony (Sb) in soils and terrestrial plants from an

565    active Sb mining area. Environ. Pollut. 159, 2427-2434.

566    Padhi, D.K., Parida, K., 2014. Facile fabrication of $\alpha$-FeOOH nanorod/RGO

567    composite: a robust photocatalyst for reduction of Cr(VI) under visible light

568    irradiation. J. Mater. Chem. A 2, 10300-10312.

569    Penke, Y. K., Anantharaman, G., Ramkumar, J., Kar, K. K. (2019). Redox synergistic

570    Mn-Al-Fe and Cu-Al-Fe ternary metal oxide nano adsorbents for arsenic

571    remediation with environmentally stable As(0) formation. J. Hazard. Mater. 364,

572    519-530.

573    Pope, J.G., McConchie, D.M., Clark, M.D., Brown, K.L., 2004. Diurnal variations in

574    the chemistry of geothermal fluids after discharge, Champagne Pool, Waiotapu.

575    New Zealand, Chem. Geol. 203, 253-272.

576    Prabhu, S.M., Park, C.M., Shahzad, A., Lee, D.S., 2019. Designed synthesis of

577    sulfide-rich bimetallic-assembled graphene oxide sheets as flexible materials and

578    self-tuning adsorption cum oxidation mechanisms of arsenic from water. J.

Mater. Chem. A 7, 12253-12265.

Qi, Z., Joshi, T.P., Liu, R., Liu, H., Qu, J., 2017. Synthesis of Ce(III)-doped $Fe_3O_4$

magnetic particles for efficient removal of antimony from aqueous solution, J.

Hazard. Mater. 329, 193-204.

Qiu, S., Yan, L., Jing, C., 2019. Simultaneous removal of arsenic and antimony from

mining wastewater using granular $TiO_2$: Batch and field column studies. J.

Environ. Sci. 75, 272-279.

Rahimi, S., Moattari, R.M., Rajabi, L., Derakhshan, A.A., Keyhani, M., 2015. Iron

oxide/hydroxide ($\alpha$, $\gamma$-FeOOH) nanoparticles as high potential adsorbents for

lead removal from polluted aquatic media. J. Ind. Eng. Chem. 23, 33-43.

Sarkar, B., Naidu, R., Megharaj, M., 2013. Simultaneous adsorption of tri- and

hexavalent chromium by organoclay mixtures. Water Air Soil Pollut. 224, 1-10,

doi: 10.1007/s11270-11013-11704-11270.

Smith, R., Knight, R., Fendorf, S., 2018. Overpumping leads to California

groundwater arsenic threat. Nat. Commun. 9, 2089-2095.

Tang, L., Feng, H., Tang, J., Zeng, G., Deng, Y., Wang, J., Liu, Y., Zhou, Y., 2017.

Treatment of arsenic in acid wastewater and river sediment by $Fe@Fe_2O_3$

nanobunches: The effect of environmental conditions and reaction mechanism.

Water Res. 117, 175-186.

Ungureanu, G., Santos, S., Boaventura, R., Botelho, C., 2015. Arsenic and antimony

in water and wastewater: overview of removal techniques with special reference

to latest advances in adsorption. J. Environ. Manag. 151, 326-342.

601 Wan, M., Shchukarev, A., Lohmayer, R., Friedrich, B.P., Peiffer, S., 2014. Occurrence

602 of surface polysulfides during the interaction between ferric(hydr) oxides and

603 aqueous sulfide. Environ. Sci. Technol. 48, 5076-5084.

604 Wang, J., Chen, Y., Zhang, Z., Ai, Y., Liu, L., Qi, L., Zhou, J., Hu, Z., Jiang, R., Bao,

605 H., Ren, S., Liang, J., Sun, H., Niu, D., Liang, Q., 2018a. Microwell Confined

606 Iron Oxide Nanoparticles in Honeycomblike Carbon Spheres for the Adsorption

607 of Sb(III) and Sequential Utilization as a Catalyst. ACS Sustainable Chem. Eng.

608 6, 12925-12934.

609 Wang, L., Wang, J., Zhang, R., Liu, X., Song, G., Chen, X., Wang, Y., Kong, J., 2016.

610 Highly efficient As(V)/Sb(V) removal by magnetic sludge composite: synthesis,

611 characterization, equilibrium, and mechanism studies. RSC Adv. 6, 42876-

612 42884.

613 Wang, L., Wang, J., Wang, Z., He, C., Lyu, W., Yan, W., Yang, L., 2018b. Enhanced

614 antimonate (Sb(V)) removal from aqueous solution by La-doped magnetic

615 biochars. Chem. Eng. J. 354, 623-632.

616 Wei, C., Ge, Z., Chu, W., Feng, R., 2015. Speciation of antimony and arsenic in the

617 soils and plants in an old antimony mine. Environ. Exp. Bot. 109, 31-39.

618 Wei, X., Liu, Q., Zhang, H., Lu, Z., Liu, J., Chen, R., Li, R., Li, Z., Liu, P., Wang, J.,

619 2017. Efficient removal of uranium(VI) from simulated seawater using

620 amidoximated polyacrylonitrile/FeOOH composites, Dalton Trans. 46, 15746-

621 15756.

622 Wei, Y., Yu, X., Liu, C., Ma, J., Wei, S., Chen, T., Yin, K., Liu, H., Luo, S., 2019.

623      Enhanced arsenite removal from water by radially porous Fe-chitosan beads:

624      Adsorption and $H_2O_2$ catalytic oxidation. J. Hazard. Mater. 373, 97-105.

625      Winship, K.A, 1987. Toxicity of antimony and its compounds, Adverse Drug React.

626      Acute Poisoning Rev. 6, 67-90.

627      Wu, D., Peng, S., Yan, K., Shao, B., Feng, Y., Zhang, Y., 2018. Enhanced As(III)

628      sequestration using sulfide-modified nanoscale zerovalent iron with a

629      characteristic core-shell structure: Sulfidation and As distribution. ACS

630      Sustainable Chem. Eng. 6, 3039-3048.

631      Xi, J., He, M., Wang, K., Zhang, G., 2013. Adsorption of antimony(III) on goethite in

632      the presence of competitive anions. J. Geochem. Explor. 132, 201-208.

633      Xu, J., Wang, Y., Weng, C., Bai, W., Jiao, Y., Kaegi, R., Lowry, G.V., 2019. Reactivity,

634      selectivity, and long-term performance of sulfidized nanoscale zerovalent iron

635      with different properties. Environ. Sci. Technol. 53, 5936-5945.

636      Yamamura, S., Bartram, J., Csanady, M., Gorchev, H.G., Redekopp, A., 2003.

637      Drinking water guidelines and standards, Arsenic, Water, and Health: the state of

638      the art. Geneva: World Health Organisation. 18.

639      Yang, H., Lu, R., Downs, R. T., Costin, G. (2006). Goethite, α-FeO (OH), from

640      single-crystal data. Acta Cryst. E 62(12), i250-i252.

641      Yang, X., Shi, Z., Yuan, M., Liu, L., 2015. Adsorption of trivalent antimony from

642      aqueous solution using graphene oxide: Kinetic and thermodynamic studies. J.

643      Chem. Eng. Data 60, 806-813.

644      Yuan, Z., Zhang, G., Lin, J., Zeng, X., Ma, X., Wang, X., Wang, S., Jia, Y., 2019. The

645    stability of Fe(III)-As(V) co-precipitate in the presence of ascorbic acid: Effect

646    of pH and Fe/As molar ratio. Chemosphere 218, 670-679.

647    Zhang, G., Ren, Z., Zhang, X., Chen, J., 2013. Nanostructured iron(III)-copper(II)

648    binary oxide: a novel adsorbent for enhanced arsenic removal from aqueous

649    solutions, Water Res. 47, 4022-4031.

650    Zhang, L., Fu, F., Tang, B., 2019. Adsorption and redox conversion behaviors of

651    Cr(VI) on goethite/carbon microspheres and akaganeite/carbon microspheres

652    composites. Chem. Eng. J. 356, 151-160.

653    Zhang, Q., Hou, Y., Wang, D., Xu, Y., Wang, H., Liu, J., Xia, L., Li, Y., Tang, N.,

654    Zheng, Q., Sun, G. (2020). Interactions of arsenic metabolism with arsenic

655    exposure and individual factors on diabetes occurrence: Baseline findings from

656    Arsenic and Non-Communicable disease cohort (AsNCD) in China. Environ.

657    Pollut. 114968.

658    Zhang, T., Wang, J., Zhang, W., Yang, C., Zhang, L., Zhu, W., Sun, J., Li, G., Li, T.,

659    Wang, J., 2019c. Amorphous Fe/Mn bimetal–organic frameworks: outer and

660    inner structural designs for efficient arsenic(III) removal. J. Mater. Chem. A 7,

661    2845-2854.

662    Zhang, X., Cheng, C., Qian, J., Lu, Z., Pan, S., Pan, B., 2017. Highly efficient water

663    decontamination by using sub-10 nm FeOOH confined within millimeter-sized

664    mesoporous polystyrene beads. Environ. Sci. Technol. 51, 9210-9218.

665    Zhang, W., Liu, C., Wang, L., Zheng, T., Ren, G., Li, J., Ma, J., Zhang, G., Song, H.,

666    Zhang, Z., Li, Z., 2019d. A novel nanostructured Fe-Ti-Mn composite oxide for

667         highly efficient arsenic removal: Preparation and performance evaluation.

668         Colloids Surf. A Physicochem. Eng. Asp. 561, 364-372.

669 Zhou, J., Zhou, X., Yang, K., Cao, Z., Wang, Z., Zhou, C., Baig, S. A., Xu, X. (2020).

670         Adsorption behavior and mechanism of arsenic on mesoporous silica modified

671         by iron-manganese binary oxide (FeMnOx/SBA-15) from aqueous systems. J.

672         Hazard. Mater. 384, 121229.

673

**Figure captions**

Fig. 1. SEM images of (a) α-FeOOH, and sulfide modified α-FeOOH samples at S/Fe

mole ratios of (b) 0.1, (c) 0.3, (d) 0.5, (e) 0.8, (f) 1.0.

Fig. 2. FTIR spectra (a), and XRD patterns (b) of α-FeOOH and sulfide-modified α-

FeOOH materials at S/Fe mole ratios of 0.1, 0.3, 0.5, 0.8 and 1.0.

Fig. 3. High resolution XPS spectra of iron (Fe 2p) (a-d), oxygen (O 1s) (e-h), and

sulfur (S 2p) (i-k) for sulfide-modified α-FeOOH materials synthesized at various

S/Fe ratios.

Fig. 4. pH versus zeta potential curves of α-FeOOH and sulfide-modified α-FeOOH

materials synthesized at various S/Fe mole ratios.

Fig. 5. Effect of pH on (a) As(V) and (b) Sb(V) adsorption by α-FeOOH and sulfide-

modified α-FeOOH materials synthesized at various S/Fe mole ratios.

Fig. 6. Effect of co-existing anions on (a) As(V) and (b) Sb(V) adsorption by α-

FeOOH and sulfide-modified α-FeOOH materials synthesized at various S/Fe mole

ratios.

Fig. 7. High-resolution XPS spectra of (a) As 3d, and (b) Sb 3d following adsorption

of As(V) and Sb(V) on α-FeOOH and sulfide-modified α-FeOOH materials

synthesized at various S/Fe mole ratios.

**Table titles**

Table 1. Pseudo-first order and pseudo-second order kinetic model parameters for As(V)

and Sb(V) adsorption on α-FeOOH and sulfide modified α-FeOOH.

Table 2. Langmuir and Freundlich isotherm model parameters for the adsorption of

As(V) and Sb(V) on α-FeOOH and sulfide modified α-FeOOH.

699  **Figures**

700
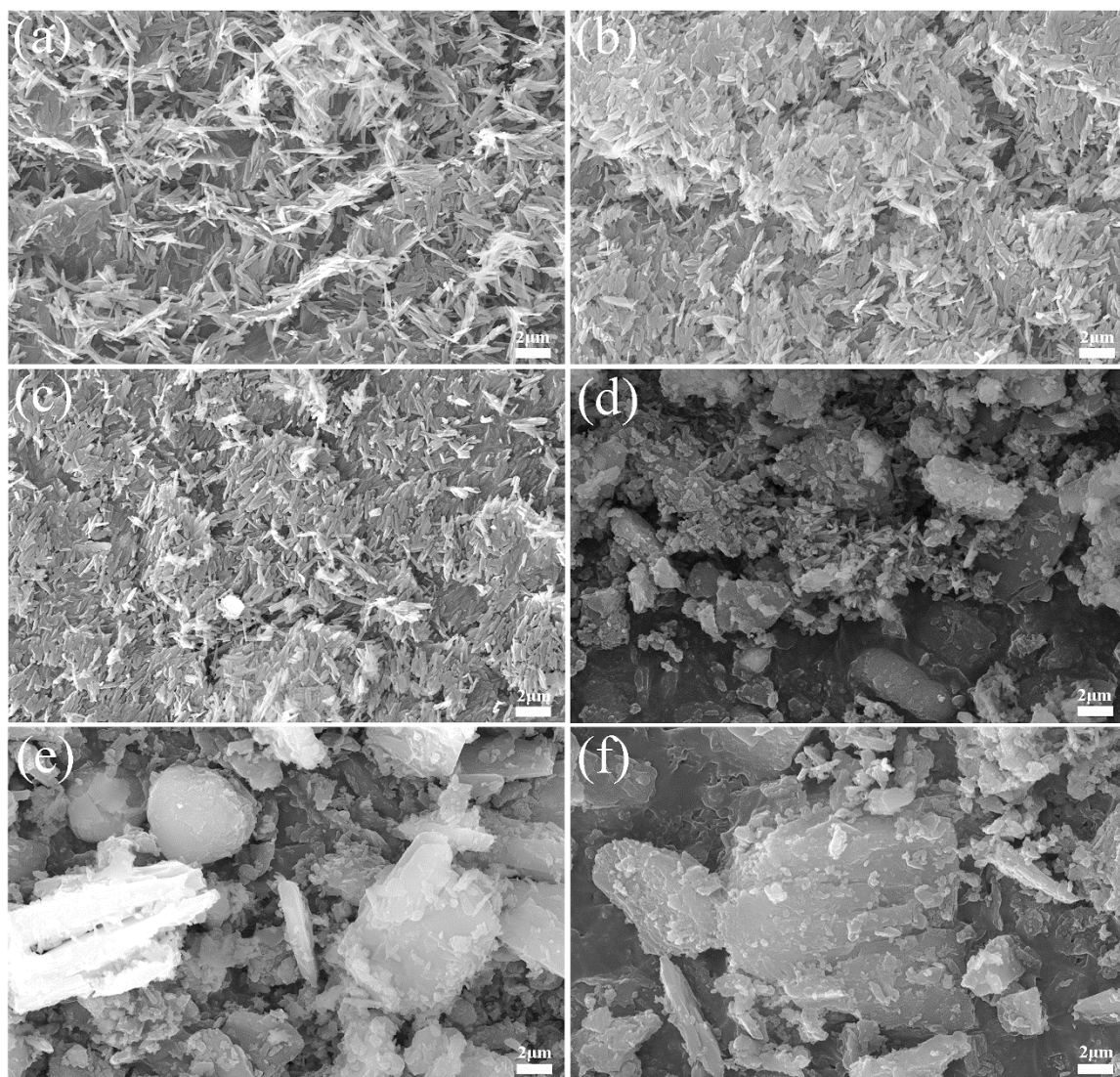


702  Fig. 1.

703
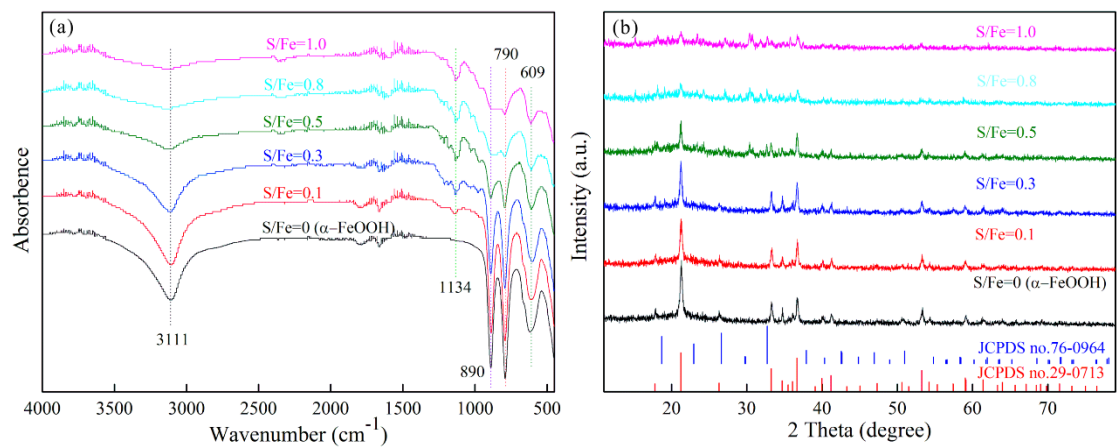
704

705     Fig. 2.

706

707
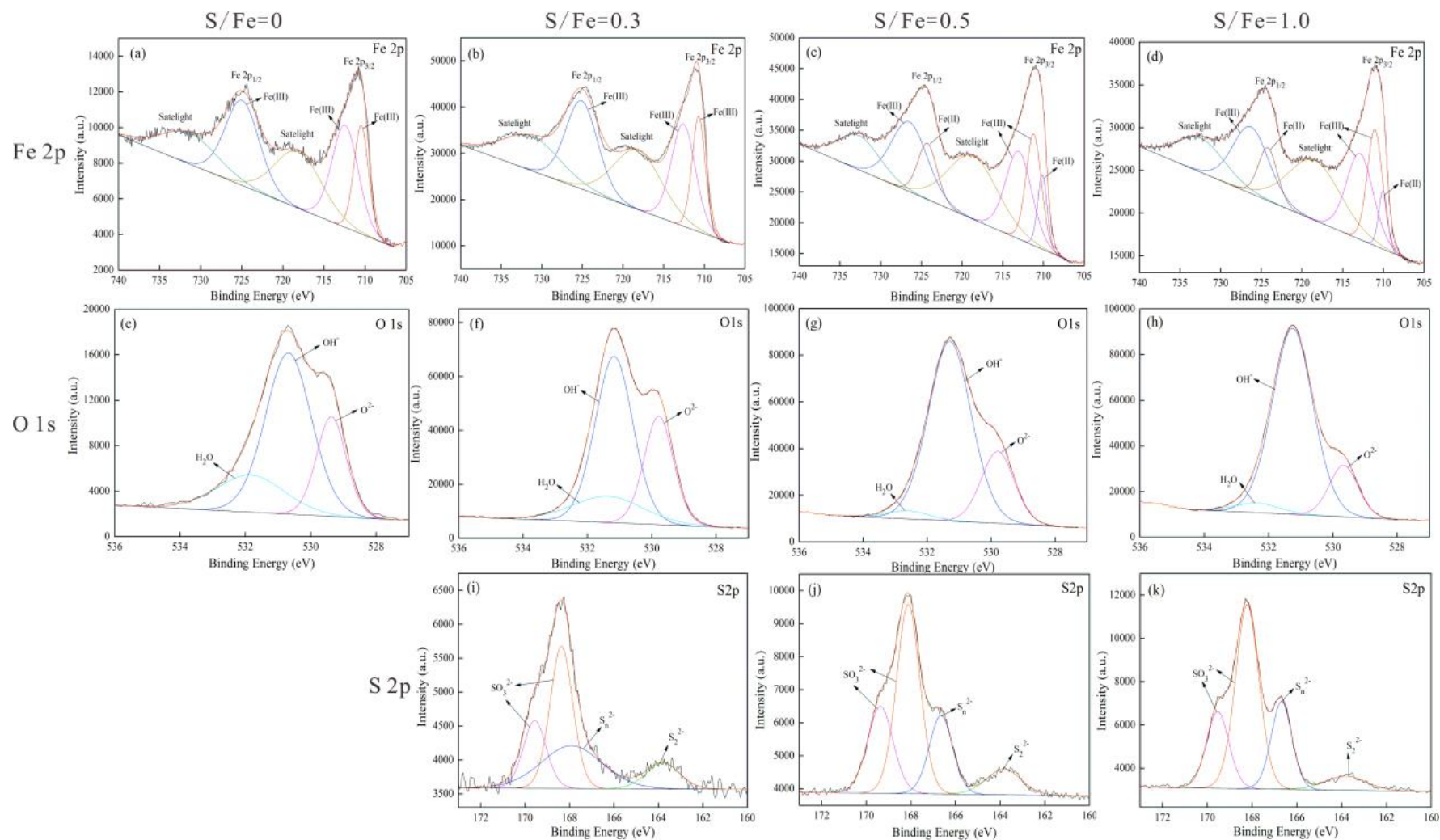
Fig. 3.
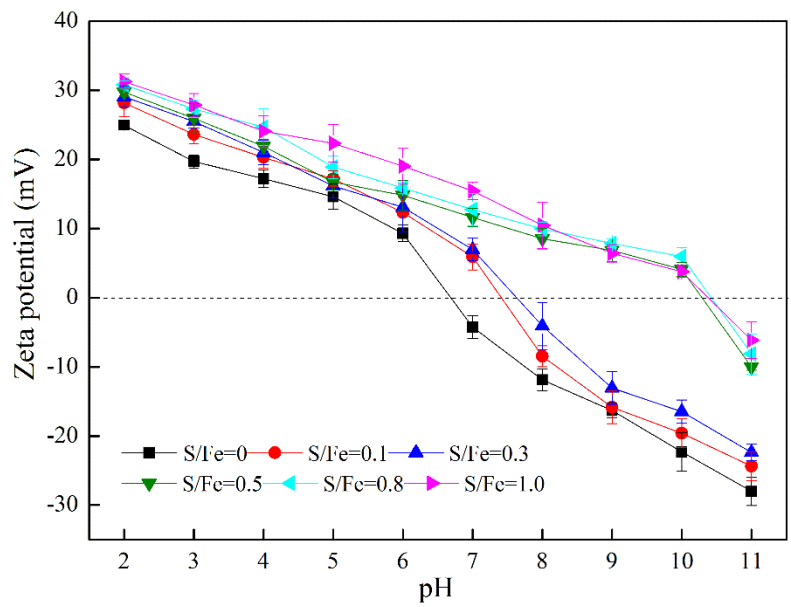
709

710    Fig. 4.

711
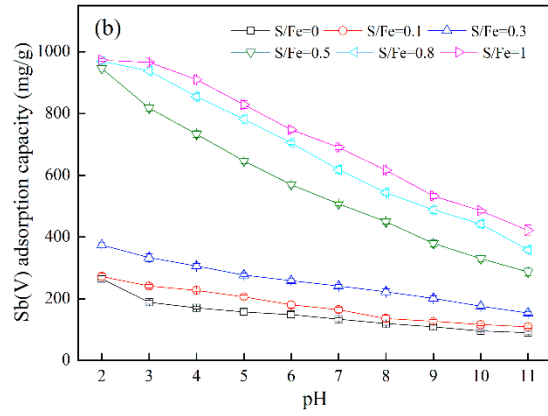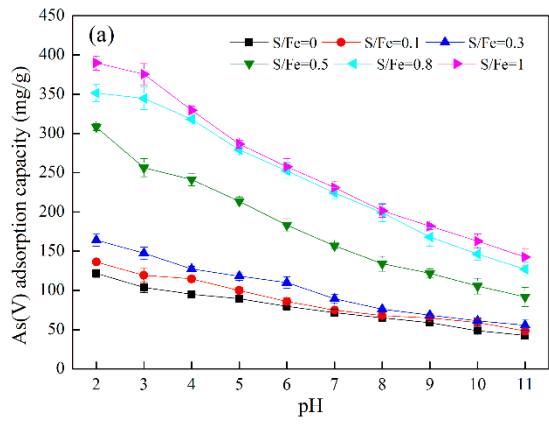
712

713    Fig. 5.

714

715
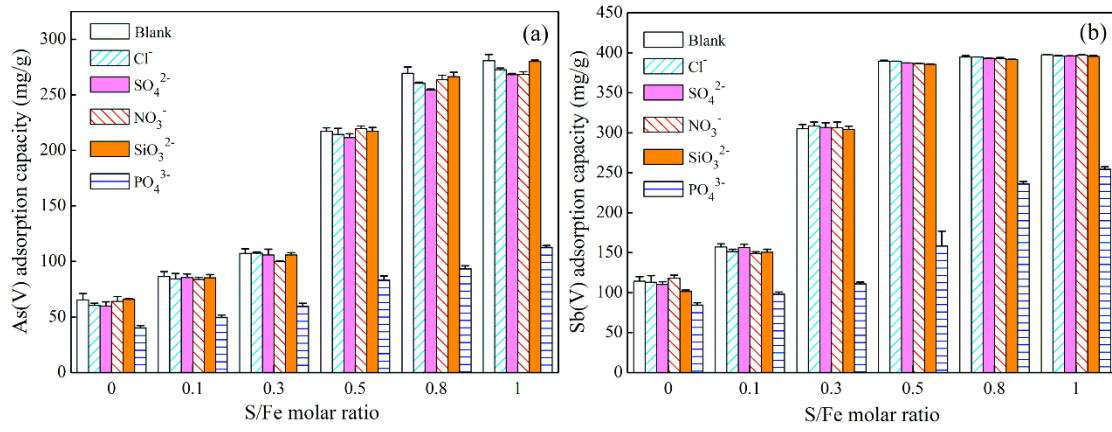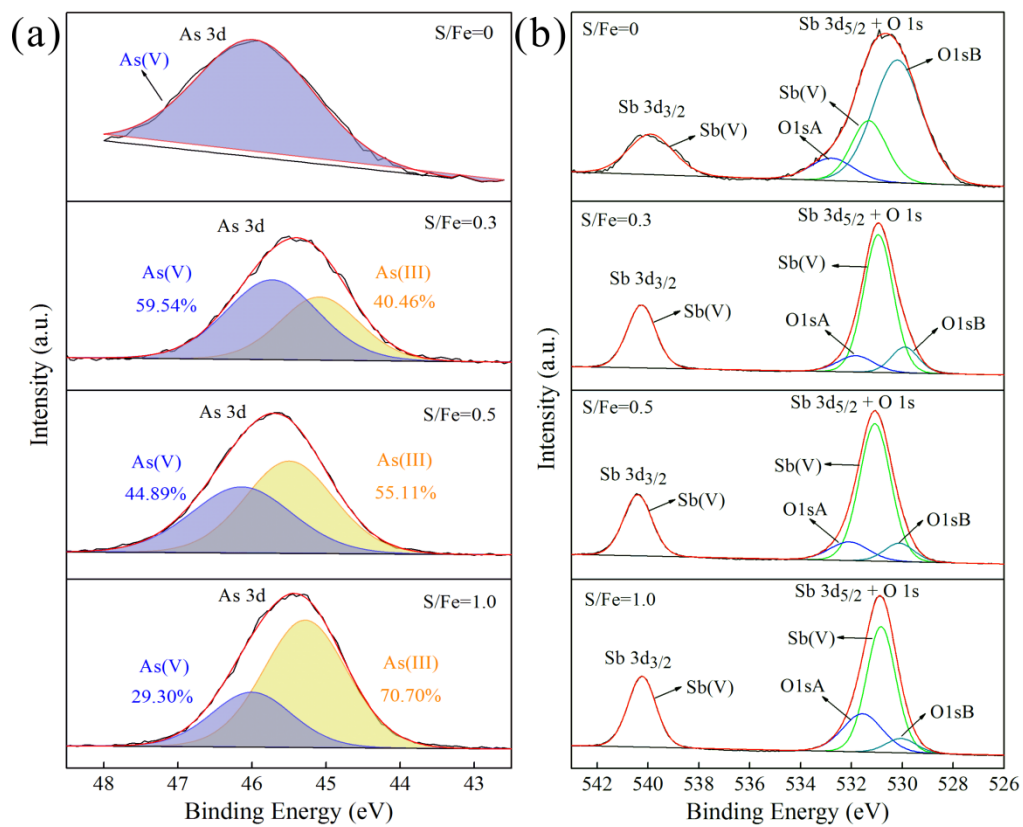
Fig. 6.

716

717

718

719    Fig. 7.

720

**Tables**

Table 1. Pseudo-first order and pseudo-second order kinetic model parameters for As(V) and Sb(V) adsorption on α-FeOOH and sulfide modified α-FeOOH.

| Adsorbate | Adsorbent | $q_{e,exp}$ | Pseudo-first order model | | | Pseudo-second order model | | |
|---|---|---|---|---|---|---|---|---|
| | | | $k_1$ (min$^{-1}$) | $q_{e,cal}$ (mg/g) | $R^2$ | $k_2$ (g/(mg min)) | $q_{e,cal}$ (mg/g) | $R^2$ |
| As(V) | S/Fe=0 | 68.4 | $1.22\times10^{-2}$ | 43.93 | 0.9903 | $7.18\times10^{-4}$ | 70.92 | 0.9972 |
| | S/Fe=0.1 | 112.8 | $8.29\times10^{-3}$ | 45.70 | 0.9717 | $7.88\times10^{-4}$ | 112.4 | 0.9968 |
| | S/Fe=0.3 | 136.0 | $1.11\times10^{-2}$ | 49.73 | 0.9662 | $8.27\times10^{-4}$ | 136.9 | 0.9980 |
| | S/Fe=0.5 | 232.8 | $6.91\times10^{-3}$ | 49.23 | 0.8702 | $8.61\times10^{-4}$ | 227.3 | 0.9986 |
| | S/Fe=0.8 | 271.0 | $1.11\times10^{-2}$ | 42.94 | 0.8850 | $1.29\times10^{-3}$ | 270.3 | 0.9998 |
| | S/Fe=1.0 | 293.6 | $5.76\times10^{-3}$ | 40.81 | 0.8119 | $1.01\times10^{-3}$ | 285.7 | 0.9989 |
| | S/Fe=0 | 132.4 | $9.21\times10^{-3}$ | 57.07 | 0.9265 | $6.58\times10^{-4}$ | 131.6 | 0.9963 |
| | S/Fe=0.1 | 237.4 | $9.67\times10^{-3}$ | 64.15 | 0.9530 | $6.44\times10^{-4}$ | 238.1 | 0.9984 |
| Sb(V) | S/Fe=0.3 | 304.2 | $1.06\times10^{-2}$ | 53.06 | 0.9438 | $9.55\times10^{-4}$ | 303.1 | 0.9996 |
| | S/Fe=0.5 | 958.9 | $1.17\times10^{-2}$ | 124.9 | 0.9118 | $4.17\times10^{-4}$ | 1000 | 0.9999 |

| | | | | | | | |
|---|---|---|---|---|---|---|---|
| S/Fe=0.8 | 981.2 | $1.59\times10^{-2}$ | 146.8 | 0.9606 | $4.35\times10^{-4}$ | 1000 | 0.9999 |
| S/Fe=1.0 | 987.2 | $2.05\times10^{-2}$ | 76.56 | 0.9171 | $1.11\times10^{-3}$ | 1000 | 1.0000 |

724
725

726 Table 2. Langmuir and Freundlich isotherm model parameters for the adsorption of As(V) and Sb(V) on α-FeOOH and sulfide modified α-FeOOH.

| Adsorbate | Adsorbent | Langmuir model | | | Freundlich model | | |
|---|---|---|---|---|---|---|---|
| | | $q_{max}$ (mg/g) | $b$ (L/mg) | $R^2$ | $K_F$ (mg/g(1/mg$^{1/n}$)) | $n$ | $R^2$ |
| As(V) | S/Fe=0 | 153.8 | $4.69 \times 10^{-3}$ | 0.9956 | 3.339 | 1.746 | 0.9904 |
| | S/Fe=0.1 | 163.9 | $6.16 \times 10^{-3}$ | 0.9954 | 4.877 | 1.858 | 0.9763 |
| | S/Fe=0.3 | 175.4 | 0.0131 | 0.9916 | 18.82 | 2.883 | 0.9971 |
| | S/Fe=0.5 | 256.4 | 0.0899 | 0.9970 | 128.2 | 8.673 | 0.9948 |
| | S/Fe=0.8 | 344.8 | 0.1014 | 0.9953 | 152.6 | 7.097 | 0.9528 |
| | S/Fe=1.0 | 384.6 | 0.0915 | 0.9938 | 161.0 | 6.873 | 0.9539 |
| Sb(V) | S/Fe=0 | 277.8 | $5.32 \times 10^{-3}$ | 0.9986 | 5.548 | 1.659 | 0.9855 |
| | S/Fe=0.1 | 294.1 | 0.0103 | 0.9916 | 15.57 | 2.128 | 0.9876 |
| | S/Fe=0.3 | 333.3 | 0.1186 | 0.9991 | 97.66 | 4.277 | 0.9003 |
| | S/Fe=0.5 | 833.3 | 0.2069 | 0.9979 | 178.69 | 2.536 | 0.9618 |
| | S/Fe=0.8 | 1000 | 0.2941 | 0.9895 | 227.77 | 2.187 | 0.9442 |
| | S/Fe=1.0 | 1111.1 | 0.4091 | 0.9932 | 283.60 | 1.951 | 0.9567 |

727

Supplementary Information for:

**Comparative removal of As(V) and Sb(V) from aqueous solution by sulfide-modified α-FeOOH**

Qiao Li[a], Rui Li[a], Xinyue Ma[a], Binoy Sarkar[b*], Xiuyun Sun[a¶], Nanthi Bolan[c]

[a] Jiangsu Key Laboratory of Chemical Pollution Control and Resources Reuse, School of Environmental and Biological Engineering, Nanjing University of Science and Technology, Nanjing 210094, China

[b] Lancaster Environment Centre, Lancaster University, Lancaster, LA1 4YQ, United Kingdom

[c] Global Centre for Environmental Remediation, University of Newcastle, Callaghan Campus, NSW 2308, Australia

*Corresponding author: Dr. Binoy Sarkar; Lancaster University; e-mail:

b.sarkar@lancaster.ac.uk; and

¶Co-corresponding author: Prof. Xiuyun Sun; Nanjing University of Science and Technology;

e-mail: sunxyun@njust.edu.cn

747 **1. SI Texts**

748 Modelling of adsorption data

749 *Adsorption kinetics*

750 Kinetic investigation is crucial for understanding the adsorption mechanism as well as the

751 equilibrium time. The pseudo-first order and pseudo-second order (Ho, 2006; Yue et al.,

752 2018) models were adopted to probe the kinetic results. The linear equations were expressed

753 as:

754 Pseudo-first-order: $\log(q_e\text{-}q_t)=\log q_e - \frac{k_1 t}{2.303}$ (SEq.1)

755 Pseudo-second-order: $\frac{t}{q_t}=\frac{1}{k_2 q_e^2}+\frac{t}{q_e}$ (SEq.2)

756 Where, $q_e$ (mg/g) and $q_t$ (mg/g) represent the adsorption capacity of As(V) or Sb(V) at

757 equilibrium and time $t$ (min), $k_1$ (min$^{-1}$) and $k_2$ (g/(mg min)) are the corresponding rate

758 constants.

759 *Adsorption isotherms*

760 Adsorption isotherms were used to explore the adsorption characteristics such as the

761 maximum adsorption as well as the adsorbate distribution between the liquid and solid

762 phases. The Langmuir and Freundlich isotherm (Lee et al., 2018; Najib and Christodoulatos,

763 2019) models were utilized for analyzing the adsorption isotherm data. The equations were

764 expressed as:

765 Langmuir isotherms model: $\frac{C_e}{q_e}=\frac{C_e}{q_{max}}+\frac{1}{bq_{max}}$ (SEq.3)

766 Freundlich isotherms model: $\log q_e=\log K_F+\frac{1}{n}\log C_e$ (SEq.4)

767 Where, $C_e$ (mg/L) and $q_e$ (mg/g) are the equilibrium concentration and equilibrium adsorption

768 capacity for As(V) or Sb(V), $q_{max}$ (mg/g) is the predicted maximum adsorption capacity of

769    sulfide-modified α-FeOOH, $b$ (L/mg) is the Langmuir constant concerning the adsorption

770    affinity and the energy of adsorption, $K_F$ (mg/g ($1/mg^{1/n}$)) is the Freundlich constant

771    concerning the capacity of adsorbent, n is the Freundlich exponential constant concerning the

772    favorability of the adsorption process.

773

774    **2.  SI Figures**

775
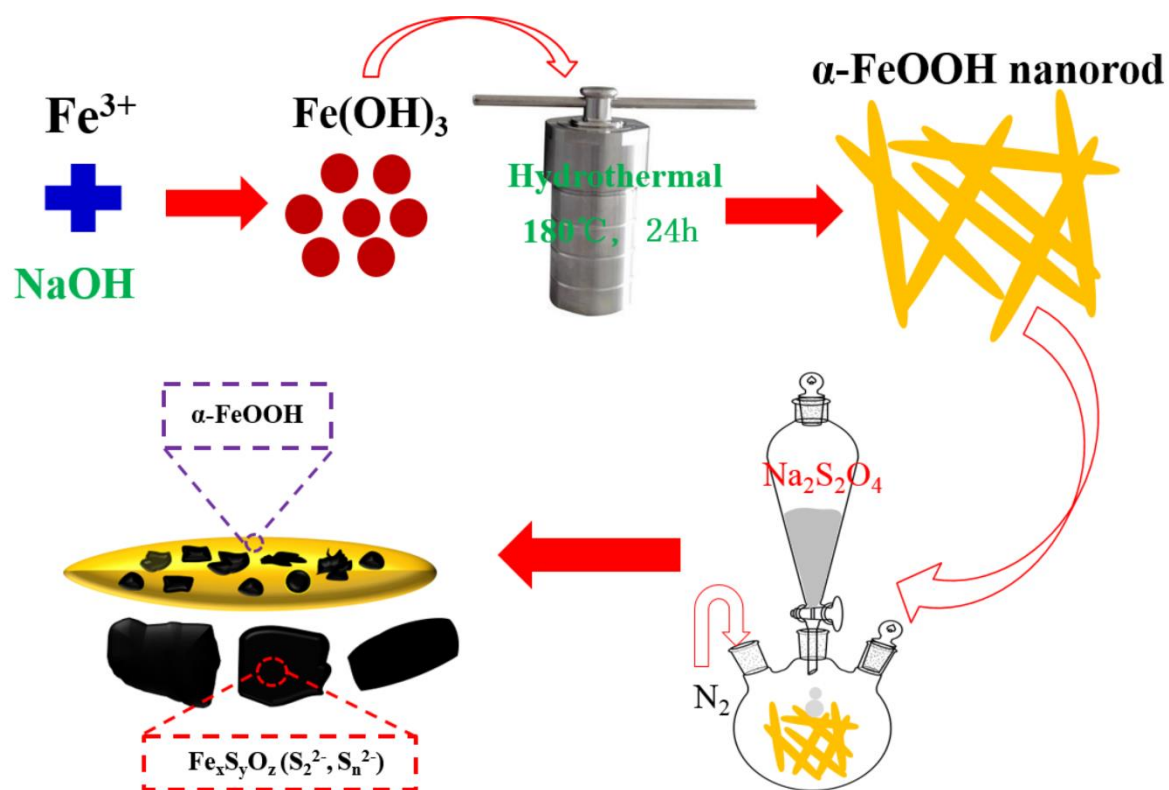


776

777    Fig. S1. Schematic for the synthesis steps of sulfide-modified α-FeOOH.

778
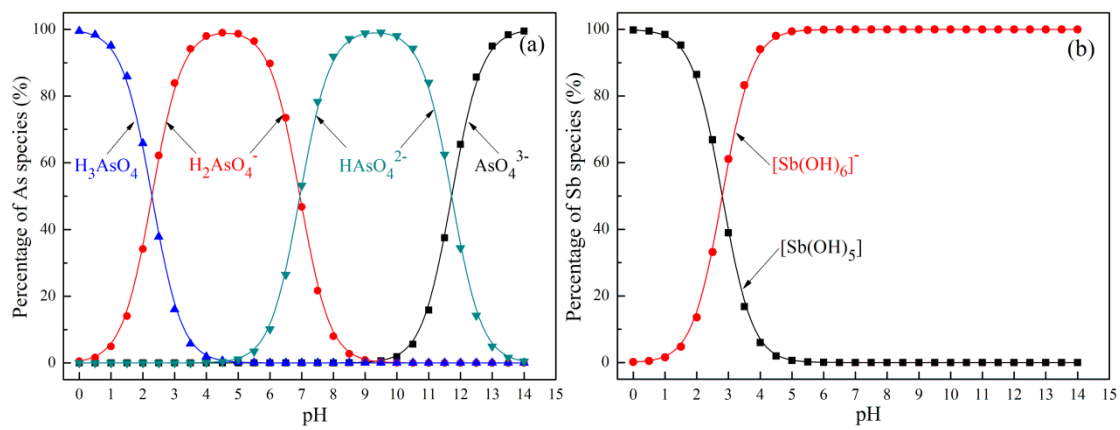
779

780　Fig. S2. As(V) and Sb(V) species distribution at different solution pH values.

781

782
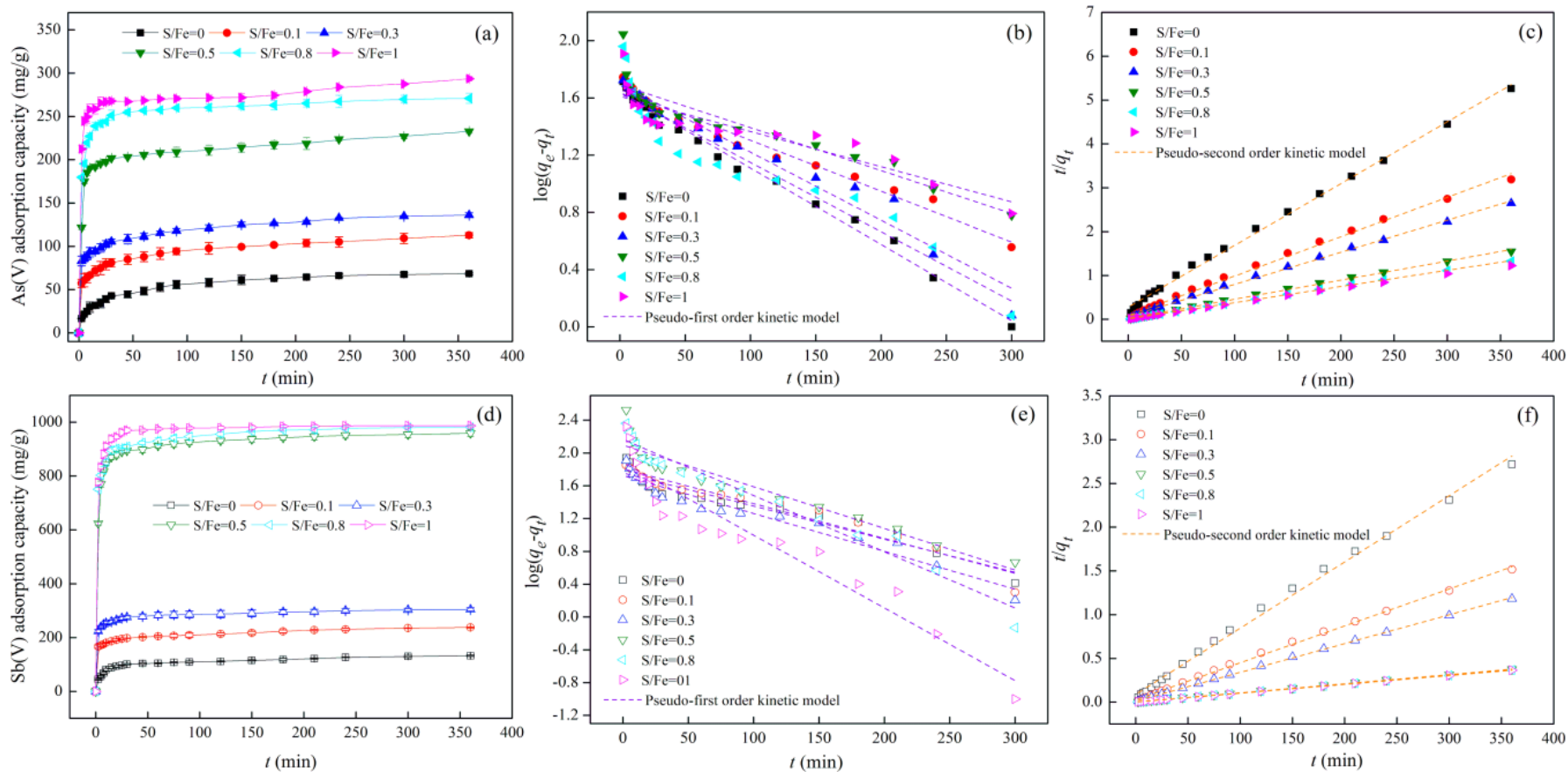
Fig. S3. Time dependence of As(V) and Sb(V) adsorption on α-FeOOH and sulfide-modified α-FeOOH materials synthesized at various S/Fe

mole ratios; (a–c) effect of contact time, pseudo-first order kinetic plot, and pseudo-second order kinetic plot for As(V) adsorption, respectively;

(d–f) effect of contact time, pseudo-first order kinetic plot, and pseudo-second order kinetic plot for Sb(V) adsorption, respectively.
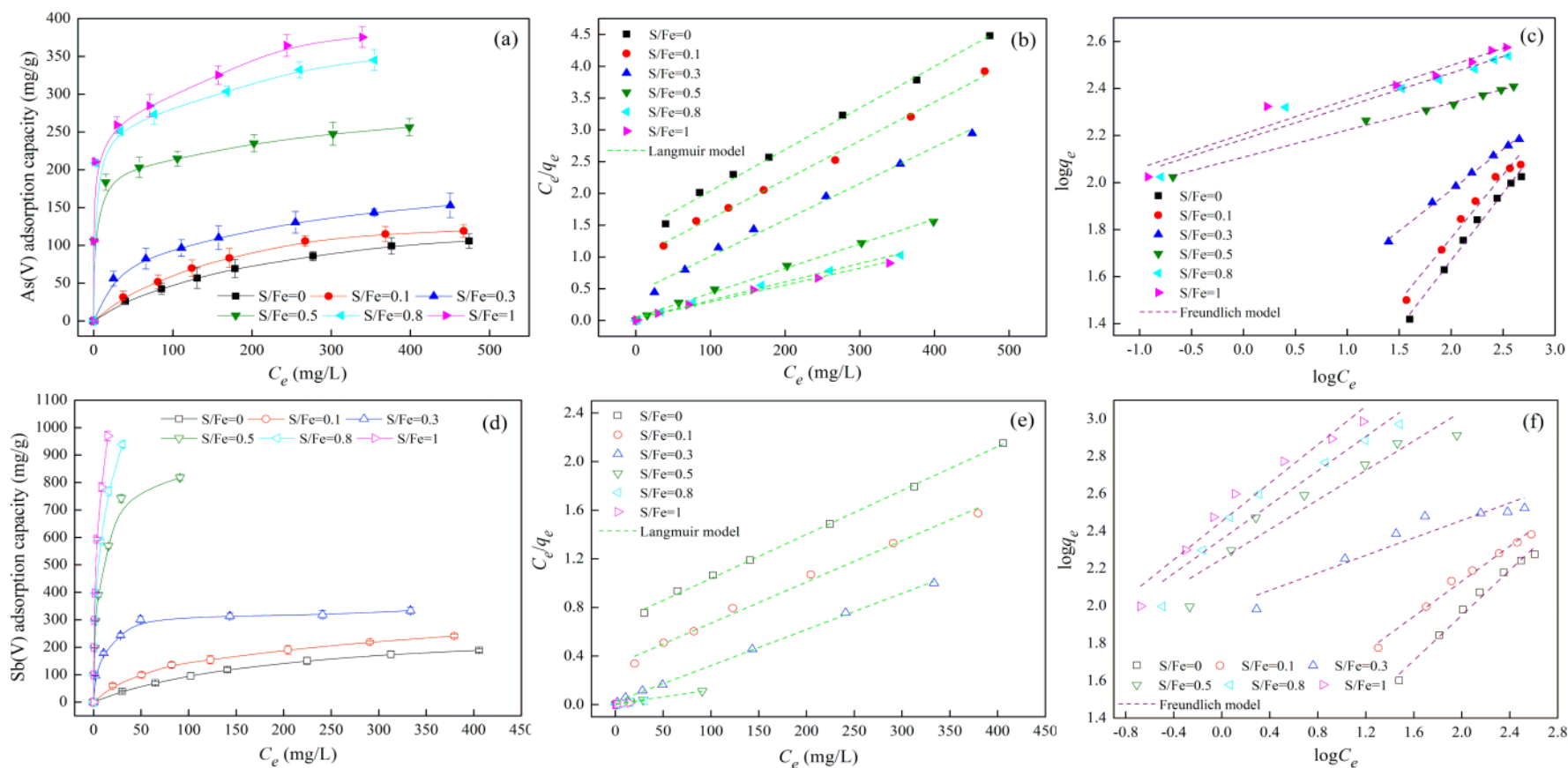
Fig. S4. Concentration dependence of As(V) and Sb(V) adsorption on α-FeOOH and sulfide-modified α-FeOOH materials synthesized at various

S/Fe mole ratios; (a–c) adsorption isotherm, Langmuir plot, and Freundlich plot for As(V) adsorption, respectively; (d–f) adsorption isotherm,

Langmuir plot, and Freundlich plot for Sb(V) adsorption, respectively.
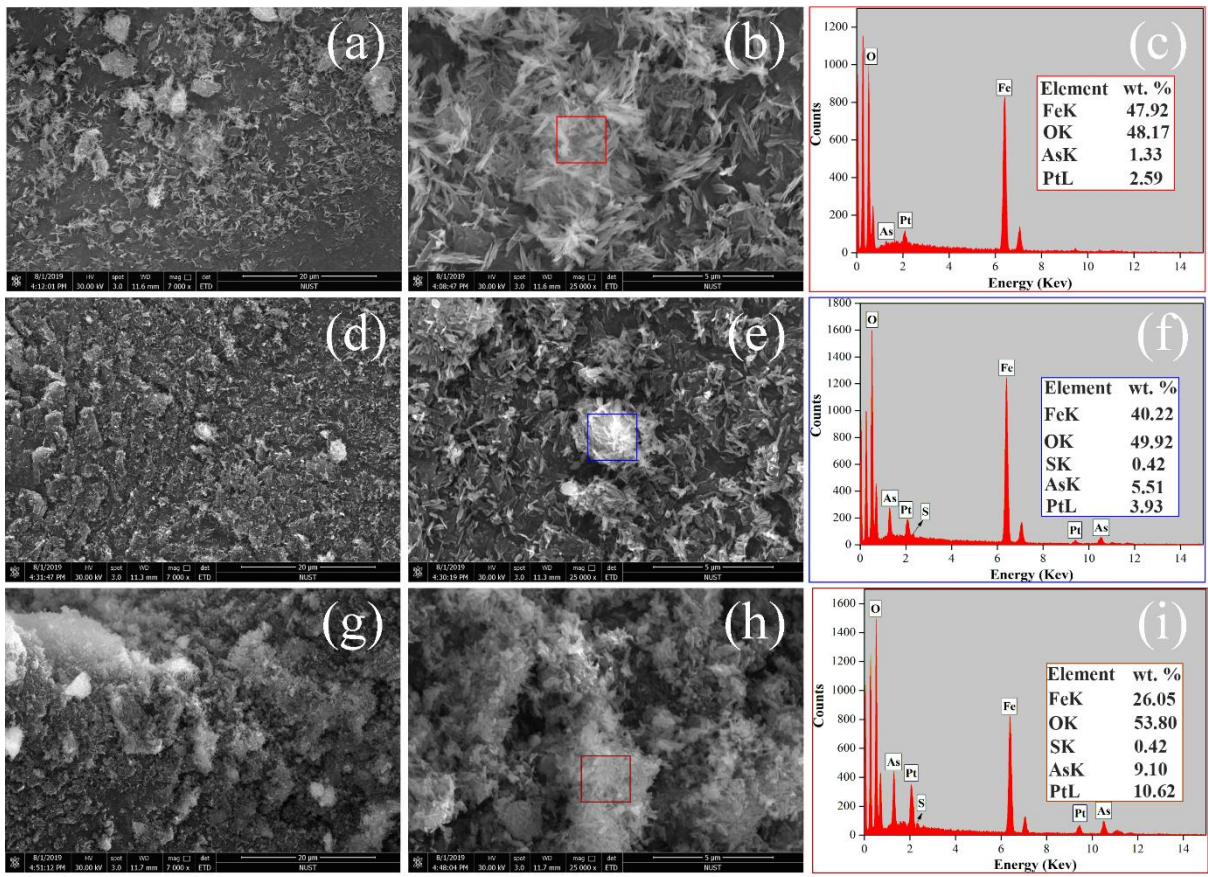
Fig. S5. SEM images and EDS spectra of adsorbents after As(V) adsorption; (a-c) S/Fe=0, (d-f) S/Fe=0.1, and (g-i) S/Fe=0.3.
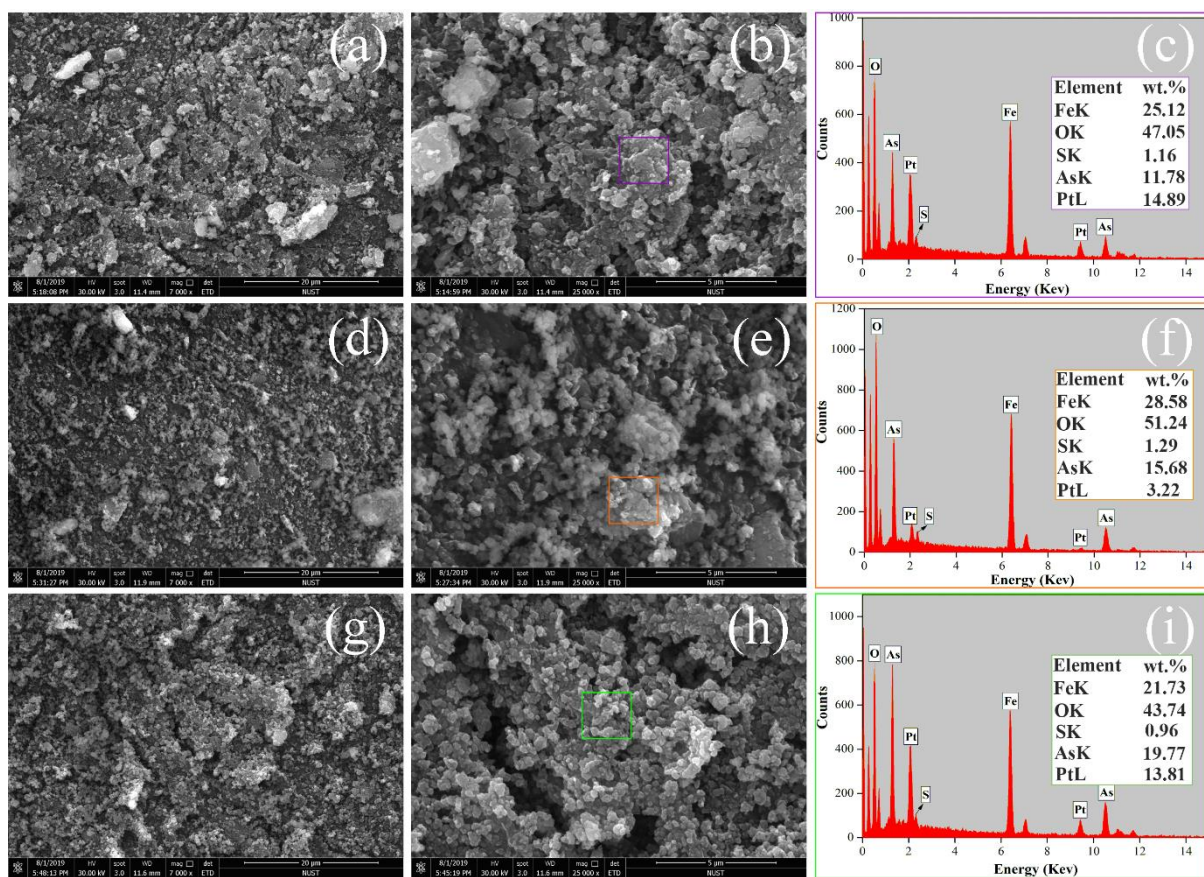
795

796    Fig. S6. SEM images and EDS spectra of adsorbents after As(V) adsorption; (a-c) S/Fe=0.5,

797    (d-f) S/Fe=0.8, and (g-i) S1.0.

798
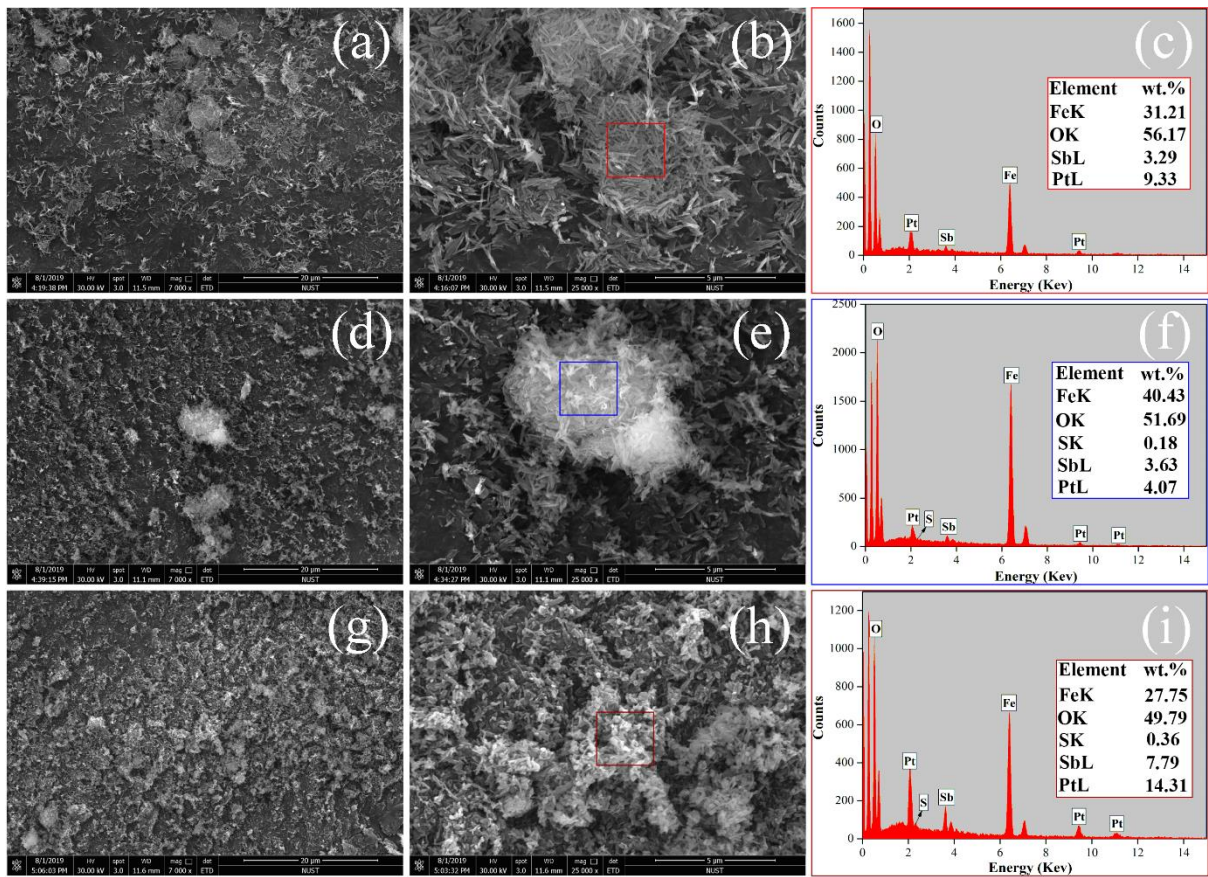
Fig. S7. SEM images and EDS spectra of adsorbents after Sb(V) adsorption; (a-c) S/Fe=0, (d-f) S/Fe=0.1, and (g-i) S/Fe=0.3.
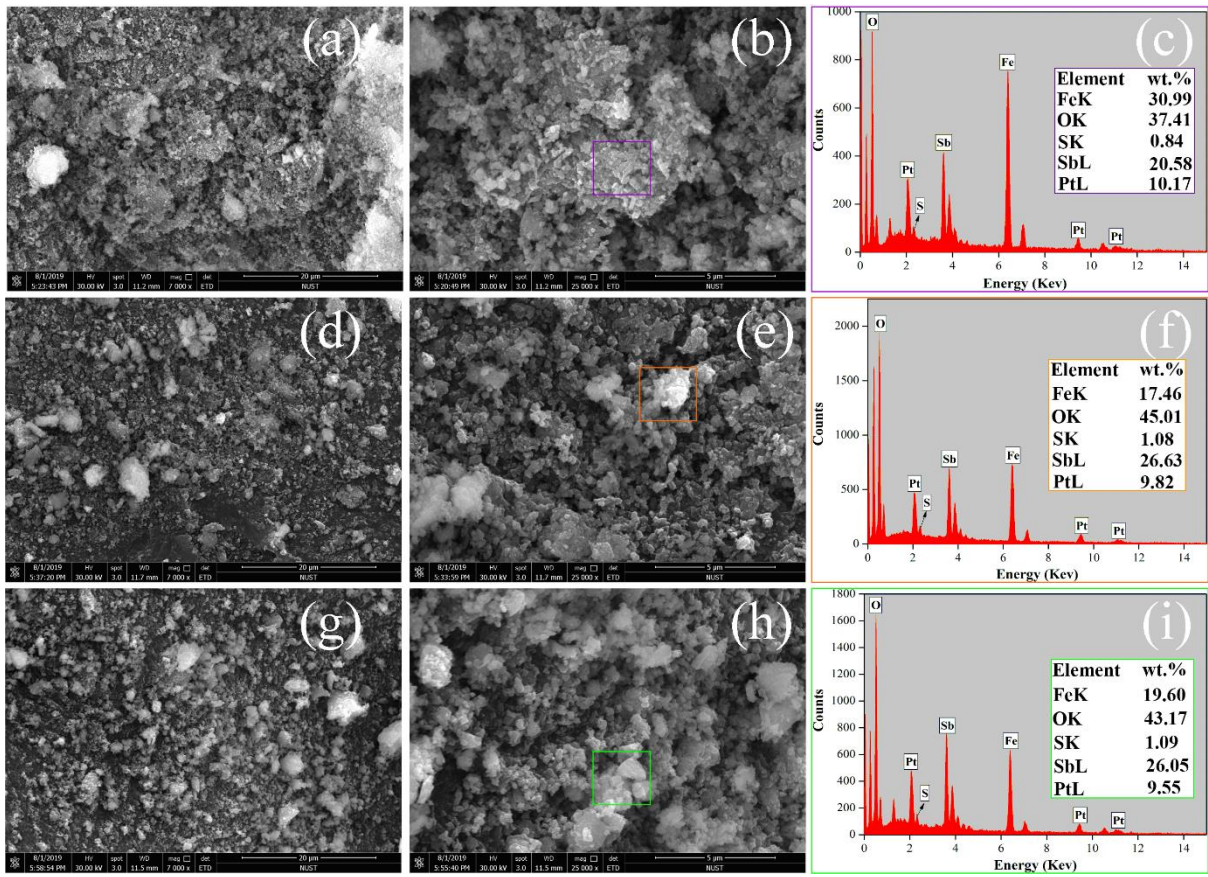
803

804 Fig. S8. SEM images and EDS spectra of adsorbents after Sb(V) adsorption; (a-c) S/Fe=0.5,

805 (d-f) S/Fe=0.8, and (g-i) S1.0.

806
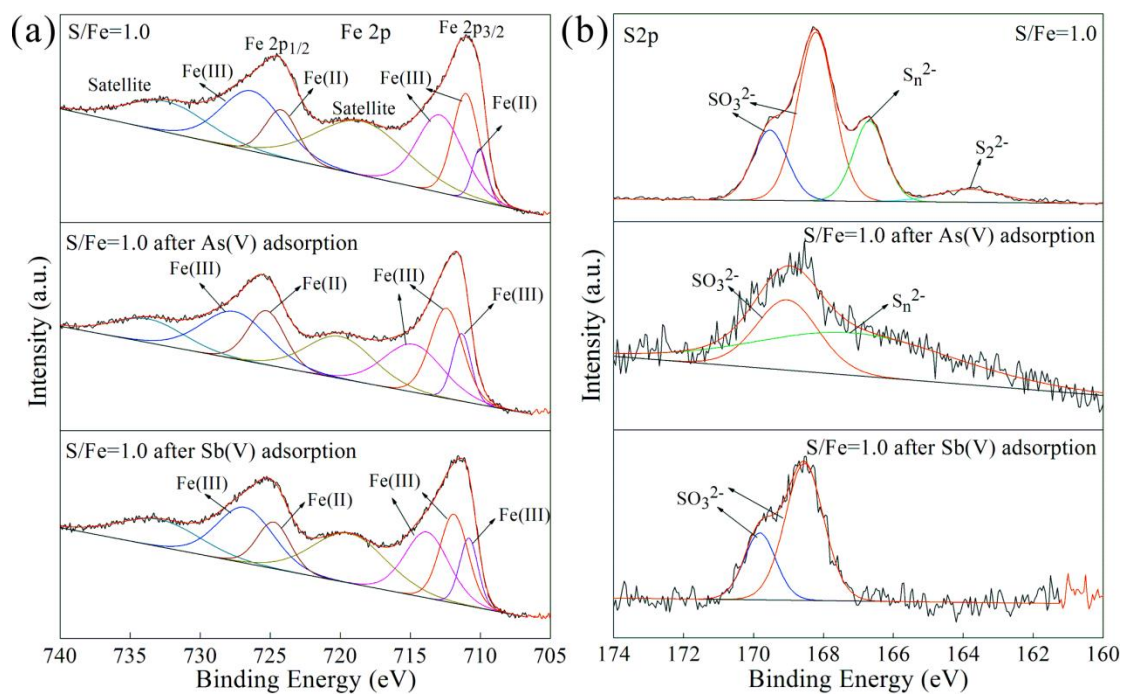
Fig. S9. High-resolution XPS spectra of Fe 2p and S 2p of sulfide-modified α-FeOOH (S/Fe=1.0).

## 3. SI Table

Table S1. Effect of sulfide modified α-FeOOH (0.5 g/L) on the solution pH during the

adsorption of As(V) and Sb(V) (500 mg/L)

| Condition | Time (h) | S/Fe ratio | | | | | |
|---|---|---|---|---|---|---|---|
| | | 0 | 0.1 | 0.3 | 0.5 | 0.8 | 1.0 |
| As(V) | 0 | 3.05 | 3.04 | 3.03 | 3.04 | 3.02 | 3.05 |
| | 4 | 3.10 | 3.03 | 3.07 | 3.06 | 3.01 | 3.08 |
| | 8 | 3.14 | 3.07 | 3.01 | 3.04 | 3.00 | 3.02 |
| | 12 | 3.10 | 3.09 | 3.03 | 3.05 | 3.02 | 3.04 |
| | 24 | 3.19 | 3.16 | 3.08 | 3.01 | 3.01 | 3.04 |
| Sb(V) | 0 | 3.02 | 3.01 | 3.03 | 3.03 | 3.02 | 3.05 |
| | 4 | 3.10 | 3.04 | 3.06 | 3.02 | 3.04 | 3.04 |
| | 8 | 3.14 | 3.07 | 3.01 | 2.99 | 3.00 | 2.98 |
| | 12 | 3.17 | 3.10 | 3.01 | 3.04 | 2.99 | 3.00 |
| | 24 | 3.17 | 3.11 | 3.03 | 3.00 | 3.01 | 2.97 |

Table S2. Comparison of maximum adsorption capacities ($q_{max}$) for As(V) and Sb(V) on

various adsorbents

| Adsorbates | Solution pH | Adsorbents | $q_{max}$(mg/g) | References |
|---|---|---|---|---|
| As(V) | 3.0 | A-60 | 205.3 | Lee et al., 2018 |
| | 2.6 | Magnetic bio-sludge | 21.3 | Wang et al., 2016 |
| | 5.0 | Fe@MesoPS | 140-190 | Zhang et al., 2017 |
| | 7.0 | Fe/Mg-MIL-88B(0.5) | 303.6 | Gu et al., 2019 |

| | 2.0 | Cellulose@iron oxide | 32.1 | Yu et al., 2013 |
|---|---|---|---|---|
| | 4.0 | GO−MnFe$_2$O$_4$ | 207 | Kumar et al., 2014 |
| | 6.0 | Sulfur-doped Fe$_3$O$_4$ | 58.38 | Liu et al., 2018 |
| | 5.0 | Biologically FeS | 234.5 | Zhou et al., 2018 |
| | 3.0 | Sulfide-modified α-FeOOH(S/Fe=1.0) | 384.6 | Present study |
| Sb(V) | 3.4 | Fe(III) treated granules | 22.6 | Wang et al., 2014 |
| | 2.6 | Magnetic bio-sludge | 43.5 | Wang et al., 2016 |
| | 7.0 | La$_{0.3}$Fe-BC | 18.9 | Wang et al., 2018 |
| | 7.0 | Mesoporous α-FeOOH | 102.7 | Xiao et al., 2019 |
| | 7.0 | Calcined Mg/Al-LDH | 303.3 | Lee et al., 2018 |
| | 2.3−9.5 | NU-1000(Zr-MOF) | 287.9 | Li et al., 2017 |
| | 2.2 | TiO$_2$ NTs | 56.30 | Zhao et al., 2019 |
| | 6.8 | RGO/Mn$_3$O$_4$ | 105.5 | Zou et al., 2016 |
| | 3.0 | Sulfide-modified α-FeOOH(S/Fe=1.0) | 1111.1 | Present study |

817

## 4. SI References

819 Gu, Y., Xie, D., Wang, Y., Qin, W., Zhang, H., Wang, G., Zhang, Y., Zhao, H. 2019. Facile

820 fabrication of composition-tunable Fe/Mg bimetal-organic frameworks for exceptional

821 arsenate removal. Chem. Eng. J. 357, 579-588.

822 Ho, Y.S. 2006. Second-order kinetic model for the sorption of cadmium onto tree fern: a

823      comparison of linear and non-linear methods. Water Res. 40(1), 119-125.

824 Kumar, S., Nair, R.R., Pillai, P.B., Gupta, S.N., Iyengar, M.A.R., Sood, A.K. 2014. Graphene

825      oxide–$MnFe_2O_4$ magnetic nanohybrids for efficient removal of lead and arsenic from

826      water. ACS Appl. Mater. Interfaces 6(20), 17426-17436.

827 Lee, C.G., Alvarez, P.J., Nam, A., Park, S.J., Do, T., Choi, U.S., Lee, S.H. 2017. Arsenic(V)

828      removal using an amine-doped acrylic ion exchange fiber: kinetic, equilibrium, and

829      regeneration studies. J. Hazard. Mater. 325, 223-229.

830 Lee, S.H., Tanaka, M., Takahashi, Y., Kim, K.W. 2018. Enhanced adsorption of arsenate and

831      antimonate by calcined Mg/Al layered double hydroxide: Investigation of comparative

832      adsorption mechanism by surface characterization. Chemosphere 211, 903-911.

833 Li, J., Li, X., Hayat, T., Alsaedi, A., Chen, C. 2017. Screening of zirconium-based metal–

834      organic frameworks for efficient simultaneous removal of antimonite (Sb(III)) and

835      antimonate (Sb(V)) from aqueous solution. ACS Sustain. Chem. Eng. 5(12), 11496-

836      11503.

837 Liu, J., Kong, L., Huang, X., Liu, M., Li, L. 2018. Removal of arsenic(V) from aqueous

838      solutions using sulfur-doped $Fe_3O_4$ nanoparticles. RSC Adv. 8(71), 40804-40812.

839 Najib, N., Christodoulatos, C. 2019. Removal of arsenic using functionalized cellulose

840      nanofibrils from aqueous solutions. J. Hazard. Mater. 367, 256-266.

841 Wang, L., Wan, C., Lee, D. J., Liu, X., Zhang, Y., Chen, X.F., Tay, J.H. 2014. Biosorption of

842      antimony (V) onto Fe (III)-treated aerobic granules. Bioresour. Technol. 158, 351-354.

843 Wang, L., Wang, J., Wang, Z., He, C., Lyu, W., Yan, W., Yang, L., 2018. Enhanced antimonate

844    (Sb(V)) removal from aqueous solution by La-doped magnetic biochars. Chem. Eng. J.

845    354, 623-632.

846    Wang, L., Wang, J., Zhang, R., Liu, X., Song, G., Chen, X., Wang, Y., Kong, J., 2016. Highly

847    efficient As(V)/Sb(V) removal by magnetic sludge composite: synthesis,

848    characterization, equilibrium, and mechanism studies. RSC Adv. 6, 42876-42884.

849    Xiao, M., Zhao, Y., Li, S. 2019. Facile synthesis of chrysanthemum-like mesoporous α-

850    FeOOH and its adsorptive behavior of antimony from aqueous solution. J. Dispersion

851    Sci. Technol. 1-9.

852    Yu, X., Tong, S., Ge, M., Zuo, J., Cao, C., Song, W. 2013. One-step synthesis of magnetic

853    composites of cellulose@ iron oxide nanoparticles for arsenic removal. J. Mater. Chem.

854    A 1(3), 959-965.

855    Yue, R., Chen, Q., Li, S., Zhang, X., Huang, Y., Feng, P. 2018. One-step synthesis of 1,6-

856    hexanediamine modified magnetic chitosan microspheres for fast and efficient removal

857    of toxic hexavalent chromium. Sci. Rep. 8(1), 1-12.

858    Zhang, X., Cheng, C., Qian, J., Lu, Z., Pan, S., Pan, B., 2017. Highly efficient water

859    decontamination by using sub-10 nm FeOOH confined within millimeter-sized

860    mesoporous polystyrene beads. Environ. Sci. Technol. 51, 9210-9218.

861    Zhao, T., Tang, Z., Zhao, X., Zhang, H., Wang, J., Wu, F., Giesy, J.P., Shi, J. 2019. Efficient

862    removal of both antimonite (Sb(III)) and antimonate (Sb(V)) from environmental water

863    using titanate nanotubes and nanoparticles. Environ. Sci. Nano 6(3), 834-850.

864    Zhou, J., Chen, S., Liu, J., Frost, R.L. 2018. Adsorption kinetic and species variation of

865    arsenic for As(V) removal by biologically mackinawite (FeS). Chem. Eng. J. 354, 237-

866    244.

867    Zou, J.P., Liu, H.L., Luo, J., Xing, Q.J., Du, H.M., Jiang, X.H., Luo, X.B., Luo, S.L., Suib,

868    S.L. 2016. Three-dimensional reduced graphene oxide coupled with $Mn_3O_4$ for highly

869    efficient removal of Sb(III) and Sb(V) from water. ACS Appl. Mater. Interfaces 8(28),

870    18140-18149.